Near-fault ground motion effects on the nonlinear response of dam-reservoir-foundation systems

Alemdar Bayraktar[†], Ahmet Can Altunişik[‡] and Barış Sevim[‡†]

Department of Civil Engineering, Karadeniz Technical University, 61080, Trabzon, Turkey

Murat Emre Kartal[‡‡]

Department of Civil Engineering, Zonguldak Karaelmas University, 67100, Zonguldak, Turkey

Temel Türker[‡‡†]

Department of Civil Engineering, Karadeniz Technical University, 61080, Trabzon, Turkey

Abstract.   Ground motions in near source region of large crustal earthquakes are significantly affected by rupture directivity and tectonic fling. These effects are the strongest at longer periods and they can have a significant impact on Engineering Structures. In this paper, it is aimed to determine near-fault ground motion effects on the nonlinear response of dams including dam-reservoir-foundation interaction. Four different types of dam, which are gravity, arch, concrete faced rockfill and clay core rockfill dams, are selected to investigate the near-fault ground motion effects on dam responses. The behavior of reservoir is taken into account by using Lagrangian approach. Strong ground motion records of Duzce (1999), Northridge (1994) and Erzincan (1992) earthquakes are selected for the analyses. Displacements, maximum and minimum principal stresses are determined by using the finite element method. The displacements and principal stresses obtained from the four different dam types subjected to these near-fault strong-ground motions are compared with each other. It is seen from the results that near-fault ground motions have different impacts on the dam types.

Keywords: arch dam; clay core rockfill dam; concrete faced rockfill dam; concrete gravity dam; dam-reservoir-foundation interaction; finite element method; near-fault strong ground motion.

1. Introduction

Near-fault ground motions are characterized by long-period (T_p) pulses, which have been seen in recent near-fault earthquakes, i.e., Landers (1992), Erzincan (1992), Northridge (1994), Kobe

† Professor, Corresponding author, E-mail: alemdar@ktu.edu.tr
‡ Research Assistant, E-mail: ahmetcan8284@hotmail.com
‡† Research Assistant, E-mail: bsevim18@hotmail.com
‡‡ Research Assistant, E-mail: murat_emre_kartal@hotmail.com
‡‡† Research Assistant, E-mail: temelturker@hotmail.com

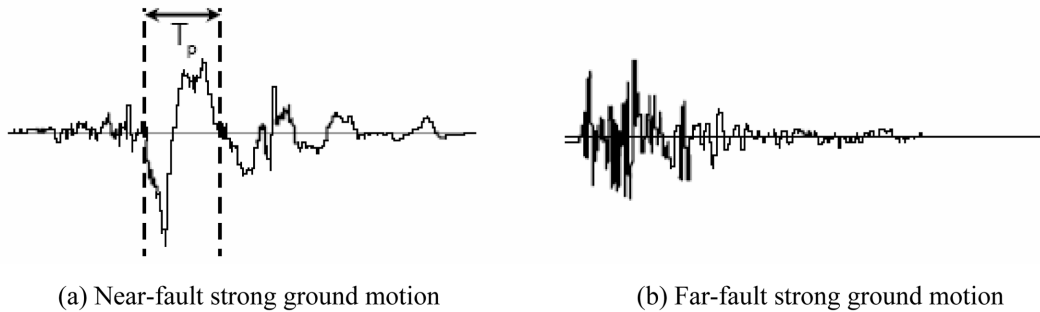(a) Near-fault strong ground motion   (b) Far-fault strong ground motion

Fig. 1 The time-histories of strong ground motion acceleration

(1995), Duzce (1999) and Chi-Chi (1999), with high peak ground velocity, which exposes the structures to high input energy in the beginning of the earthquake. Comparison of near-fault strong ground motions with far-fault strong ground motions is shown in Fig. 1. These pulses are strongly influenced by the orientation of the fault, the direction of slip on the fault and the location of the recording station relative to the fault, which is termed as 'directivity effect' due to the propagation of the rupture toward the recording site (Agrawal and He 2002, Aki 1968, Archuleta and Hartzell 1981, Somerville *et al.* 1997, Bray and Marek 2004, Somerville 2003, Megawati *et al.* 2001, Wang *et al.* 2002, Pulido and Kubo 2004).

The effects of near-fault ground motion on many civil engineering structures such as buildings, tunnels, bridges, nuclear station etc. have been investigated in many recent studies (Makris 1997, Chopra and Chintanapakdee 2001, Bertero *et al.* 1978, Anderson and Bertero 1987, Hall *et al.* 1995, Corigliano *et al.* 2006, Ozturk 2006, Ghahari *et al.* 2006, Galal and Ghobarah 2006, Dicleli and Buddaram 2006, Liao *et al.* 2004). It can be seen clearly from these studies that the importance of this subject on the response of the structures has been highlighted. Dynamic responses of dam-reservoir-foundation systems have been investigated using the Eulerian and Lagrangian approaches by many researches (Bayraktar *et al.* 2005, Bayraktar *et al.* 2005, Zangar and Haefei 1952, Zienkiewicz and Nath 1963, Chopra 1968, Finn and Varolu 1973, Saini *et al.* 1978, Chopra and Chakrabarti 1981, Fenves and Chopra 1984, Greeves and Dumanolu 1989, Singhal 1991, Greeves 1991, Calayr *et al.* 1996, Bayraktar *et al.* 1996, Araujo and Awruch 1998, Fenves and Chopra 1984). In Eulerian approach, the displacements are the variables in the structure; the pressures are the variables in the fluid. However, in Lagrangian approach, the displacements are the variables in both the fluid and the structure. So that there is no need any extra interface equations. For that reason, compatibility and equilibrium are automatically satisfied at the nodes along the interfaces between the fluid and structure. However, there is not sufficient research about the effects of near-fault ground motions on dam responses.

In this study, the effects of the near-fault strong ground motion on the nonlinear response of dams including dam-reservoir-foundation interaction are investigated by using Lagrangian approach. For this purpose, concrete gravity, Type-5 arch, concrete faced rockfill, and clay core rockfill dams are selected to examine the responses of the different type of dams subjected to near-fault strong ground motion. The strong ground motions of the Duzce (1999), Northridge (1994) and Erzincan (1992) earthquakes recorded near-fault are considered in the analyses. The ANSYS finite element program was selected in the analyses (ANSYS 2003) for its ability to include solid and fluid elements contained 2D and 3D, fluid-structure interactions, material nonlinearity and transient analysis.

2. Formulation of dam-reservoir-foundation interaction by lagrangian approach

The formulation of the fluid system based on Lagrangian approach is given according to references (Calayr *et al.* 1996, Wilson and Khalvati 1983, Calayr 1994). In this approach, the fluid is assumed to be linearly elastic, inviscid and with irrotational flow field. For a general three-dimensional fluid, stress-strain relationships can be written in matrix form as follows

$$
\begin{Bmatrix} P \\ P_x \\ P_y \\ P_z \end{Bmatrix} = \begin{bmatrix} C_{11} & 0 & 0 & 0 \\ 0 & C_{22} & 0 & 0 \\ 0 & 0 & C_{33} & 0 \\ 0 & 0 & 0 & C_{44} \end{bmatrix} \begin{Bmatrix} \varepsilon_v \\ w_x \\ w_y \\ w_z \end{Bmatrix}
\tag{1}
$$

In this equation, P_x, P_y, P_z are the rotational stresses; C_{22}, C_{33}, C_{44} are the constraint parameters and w_x, w_y and w_z are the rotations about the cartesian axis x, y and z, respectively, where P, C_{11}, and ε_v are the pressures which are equal to mean stresses, the bulk modulus and the volumetric strains of the fluid, respectively. Since irrotationality of the fluid is considered like penalty methods (Bathe 1996), rotations and constraint parameters are included in the stress-strain Eq. (1) of the fluid.

In this study, the equations of motion of the fluid system were obtained using potential and kinetic energy principles. Using the finite element method, the total strain energy of the fluid system may be written as

$$
\pi_e = \frac{1}{2} \mathbf{U}_f^T \mathbf{K}_f \mathbf{U}_f
\tag{2}
$$

where $\mathbf{U}_f$ and $\mathbf{K}_f$ are the vectors of nodal displacements and the stiffness matrix of the fluid system, respectively. $\mathbf{K}_f$ is obtained by summing the stiffness matrices of the fluid elements in the following

$$
\begin{aligned}
\mathbf{K}_f &= \sum \mathbf{K}_f^e \\
\mathbf{K}_f^e &= \int_V \mathbf{B}_f^{eT} \mathbf{C}_f \mathbf{B}_f^e dV^e
\end{aligned} \Bigg\}
\tag{3}
$$

where $\mathbf{C}_f$ is the elasticity matrix consisting of diagonal terms in Eq. (1). $\mathbf{B}_f^e$ is the strain-displacement matrix of the fluid element.

An important behavior of fluid systems is the ability to displace without a change in volume. For reservoir and storage tanks, this movement is known as sloshing waves in which the displacement is in the vertical direction. The increase in the potential energy of the system due to the free surface motion can be written as

$$
\pi_s = \frac{1}{2} \mathbf{U}_{sf}^T \mathbf{S}_f \mathbf{U}_{sf}
\tag{4}
$$

where $\mathbf{U}_{sf}$ and $\mathbf{S}_f$ are the vertical nodal displacement vector and the stiffness matrix of the free surface of the fluid system, respectively. $\mathbf{S}_f$ is obtained by the sum of the stiffness matrices of the free surface fluid elements in the following

$$
\begin{aligned}
\mathbf{S}_f &= \sum \mathbf{S}_f^e \\
\mathbf{S}_f^e &= \rho_f g \int_A \mathbf{h}_s^T \mathbf{h}_s dA^e
\end{aligned} \Bigg\}
\tag{5}
$$

where $\mathbf{h}_s$ is the vector consisting of interpolation functions of the free surface fluid element. r_f and g are the mass density of the fluid and the acceleration due to gravity, respectively. Also, the kinetic energy of the system can be written as

$$T = \frac{1}{2}\dot{\mathbf{U}}_f^T \mathbf{M}_f \dot{\mathbf{U}}_f \tag{6}$$

where $\dot{\mathbf{U}}_f$ and $\mathbf{M}_f$ are the nodal velocity vector and the mass matrix of the fluid system, respectively. $\mathbf{M}_f$ can be obtained by summing the mass matrices of the fluid elements in the following

$$\left.\begin{aligned} \mathbf{M}_f &= \sum \mathbf{M}_f^e \\ \mathbf{M}_f^e &= \rho_f \int_V \mathbf{H}^T \mathbf{H} \, dV^e \end{aligned}\right\} \tag{7}$$

where $\mathbf{H}$ is the matrix consisting of interpolation functions of the fluid element. If Eqs. (2), (4) and (6) are combined using the Lagrange's equation (Clough and Penzien 1975); the following set of equations is obtained

$$\mathbf{M}_f \ddot{\mathbf{U}}_f + \mathbf{M}_f^* \mathbf{U}_f = \mathbf{R}_f \tag{8}$$

where $\mathbf{M}_f^*$, $\ddot{\mathbf{U}}_f$ and $\mathbf{R}_f$ are the system stiffness matrix including the free surface stiffness, the nodal acceleration vector and time-varying nodal force vector for the fluid system, respectively. In the formation of the fluid element matrices, reduced integration orders were utilized.

The equations of motion of the fluid system, Eq. (8), have a similar form with those of the structural system. To obtain the coupled equations of the fluid-structure system, the determination of the interface condition is required. Because the fluid is assumed to be inviscid, only the displacement in the normal direction to the interface is continuous at the interface of the system. Assuming that the positive face is the structure and the negative face is the fluid, the boundary condition at the fluid-structure interface is

$$U_n^- = U_n^+ \tag{9}$$

where U_n is the normal component of the interface displacement (Akkas *et al.* 1979). Using the interface condition, the equations of motion of the coupled system to ground motion including damping effects are given by

$$\mathbf{M}_c \ddot{\mathbf{U}}_c + \mathbf{C}_c \dot{\mathbf{U}}_c + \mathbf{K}_c \mathbf{U}_c = \mathbf{R}_c \tag{10}$$

in which $\mathbf{M}_c$, $\mathbf{C}_c$, and $\mathbf{K}_c$ are the mass, damping and stiffness matrices for the coupled system, respectively. $\mathbf{U}_c$, $\dot{\mathbf{U}}_c$, $\ddot{\mathbf{U}}_c$ and $\mathbf{R}_c$ are the vectors of the displacements, velocities, accelerations and external loads of the coupled system, respectively.

3. Near-fault ground motions

The DUZCE/DZC270 component of DUZCE station recorded during the Duzce Earthquake in

1999, the ERZIKAN/ERZ-NS component of 95 Erzincan station recorded during the Erzincan Earthquake in 1992, and the NORTHR/RRS318 component of 77 Rinaldi Receiving station recorded during the Northridge Earthquake in 1994 are used as ground motions. The time-histories of accelerations and velocities of these records are indicated in Figs. 2, 3. The strong motion records are obtained from the PEER Strong Motion Database (PEER 2006). The databases have information on the site conditions and the soil type for the instrument locations. When selecting the near-fault ground motions it is considered that the ground motions have similar properties such as near peak acceleration value to compare the effects different near-fault ground motion on dam response. Table 1 presents the list the parameters of the ground motion records.
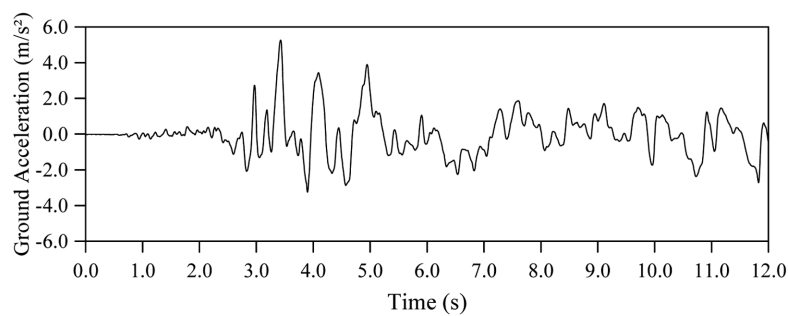
(a) The time-histories of strong ground motion acceleration subjected to Duzce 1999
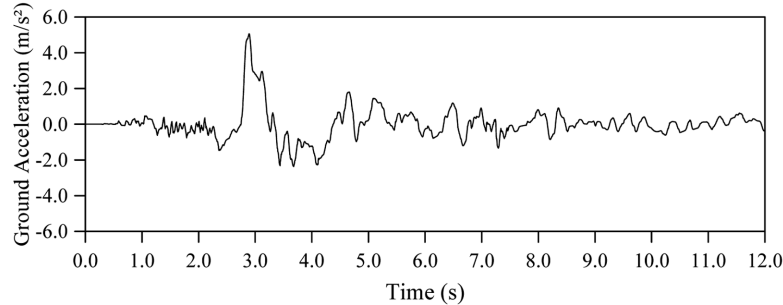
(b) The time-histories of strong ground motion acceleration subjected to Erzincan 1992
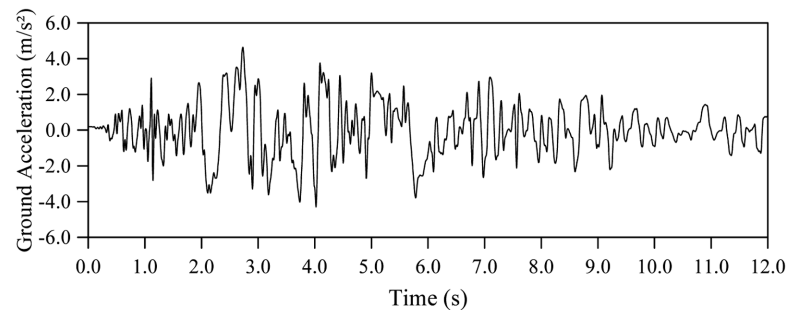
(c) The time-histories of strong ground motion acceleration subjected to Northridge 1994

Fig. 2 The time-histories of selected strong ground motion acceleration
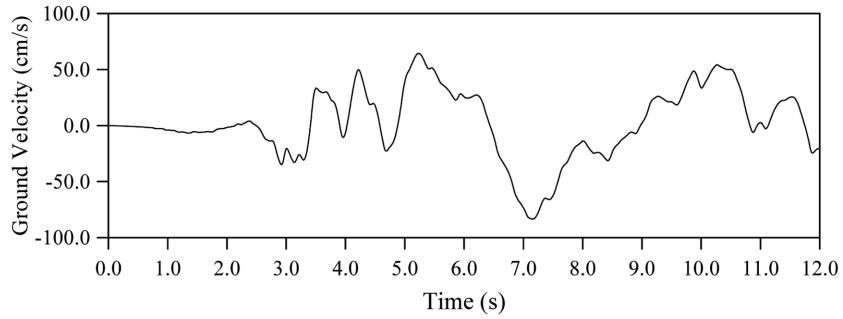
(a) The time-histories of strong ground motion velocities subjected to Duzce 1999
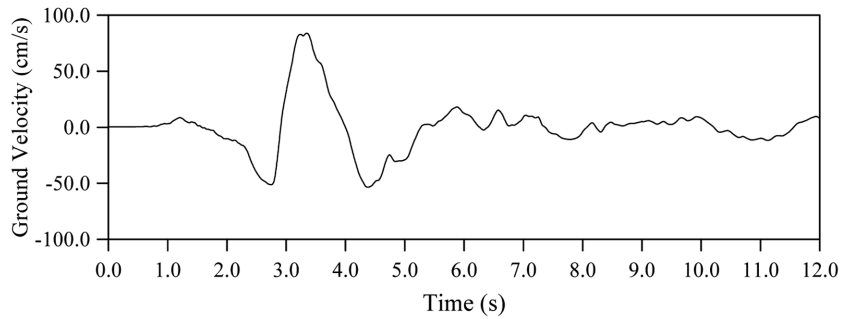
(b) The time-histories of strong ground motion velocities subjected to Erzincan 1992
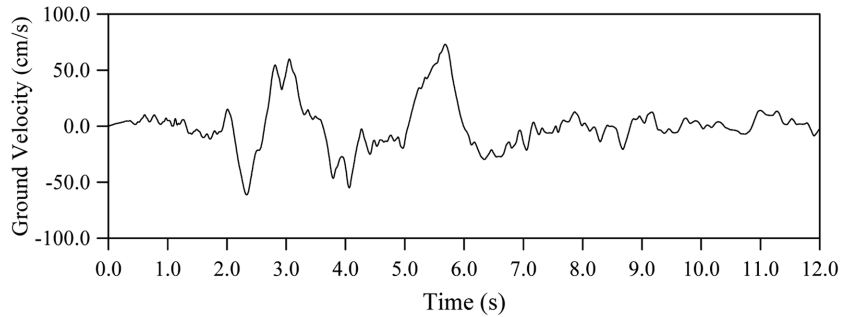
(c) The time-histories of strong ground motion velocities subjected to Northridge 1994

Fig. 3 The time-histories of selected strong ground motion velocities

Table 1 Strong motion records selected for consideration

No	Near-fault strong-ground motions				
	Earthquake	M	D, km	Site (*)	Peak Acc.
1	Duzce	7.1	8.2	D	0.535 g
2	Erzincan	6.9	2.0	D	0.515 g
3	Northridge	6.7	7.1	C	0.472 g

(*) Geomatrix site classification; see Table 2.

Table 2 Geomatrix classification of geotechnical subsurface characteristics

Type	Geomatrix classification of geotechnical subsurface characteristics	
	Site name	Description of instrument site
C	Deep narrow soil	Soil profile at least 20 m thick overlying rock, in a narrow canyon or valley no more than several km wide
D	Deep broad soil	Soil profile at least 20 m thick overlying rock, in a broad valley
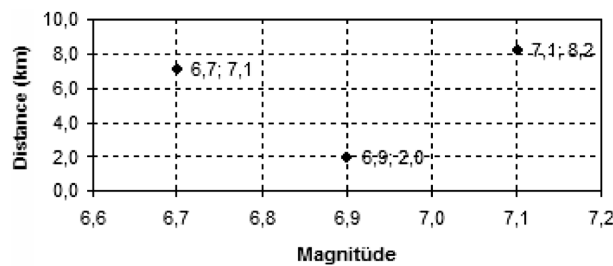
Fig. 4 Magnitude-distance distribution

The Duzce, Turkey (1999), earthquake was recorded during the 7.1 magnitude earthquake; that magnitude was the highest considered in this study. The distance of the recording site from the source ranged from 2.0-8.2 km. A scatter plot of the magnitude-distance pairs for the strong ground motion records is shown in Fig. 4. All of the records were obtained from sites with epicentral distances of less than 10 km.

4. Numerical example

The focus of this paper is to perform nonlinear transient analysis of the dams and to determine near-fault strong ground motion effects on response of dams including dam-reservoir-foundation by using the Lagrangian (displacement-based) approach. For this purpose, four different finite elements models belong to the Folsom gravity dam, Type-5 arch dam, Torul concrete faced rockfill dam, and Kose clay core rockfill dam were selected as examples.

The finite element method is used to investigate the nonlinear dynamic response of dams and determine the near-fault effect on dam. The dams and foundations are represented by solid elements, and the reservoirs are represented by fluid elements in all dam models. Plane42 element is used to represent the dam and foundation, and Fluid79 element is used to represent the reservoir in the modeling of Folsom gravity dam, Torul concrete faced rockfill dam, and Kose clay core rockfill dam. In addition, Solid45 element is used to represent the dam, the foundation, and the Fluid 80 element is used for reservoir at Type-5 arch dam. In the selection of the elements, it is considered stress-strain relationships that formulation of the fluid elements was suitable with the Lagrangian approach given in Eqs. (1)-(8). In nonlinear transient analysis of dam-reservoir-foundation systems, Drucker-Prager criteria for dam body are taken into account in this study. Massless foundation is used in all dam-reservoir-foundation models. At the reservoir-dam and reservoir-foundation interface, length of coupling element was chosen as 0.001 m. The main objective of the couplings is hold equal to the displacements between two reciprocal nodes. The length in the upstream direction

is taken to be as much as three times the dam height in all models. It is assumed that the reservoir has constant depth. In addition, the foundation depths are taken into account as much as the dam heights. In the upstream direction, foundation length is considered as the reservoir length and in the downstream direction, foundation length is considered as the dam height. Element matrices are computed using the Gauss numerical integration technique (Bathe 1996). The Newmark method is used in the solution of the equation of motions. Rayleigh damping is considered in the analyses and the damping ratio is selected as 5%.

4.1 Earthquake response of gravity dam

Folsom Dam, located approximately 37 km northeast of Sacramento, CA, was constructed in 1956 by the U.S. Army Corps of Engineers and is now operated by the U.S. Bureau of Reclamation (Fig. 5). The reservoir has been used for flood control, irrigation, and power-generation purposes. The dam crest is 427 m long and 11m wide, and the maximum height and base width are 104 m and 82 m, respectively. The dam consists of 28 monoliths, 15 m wide each, constructed in 1,5 m
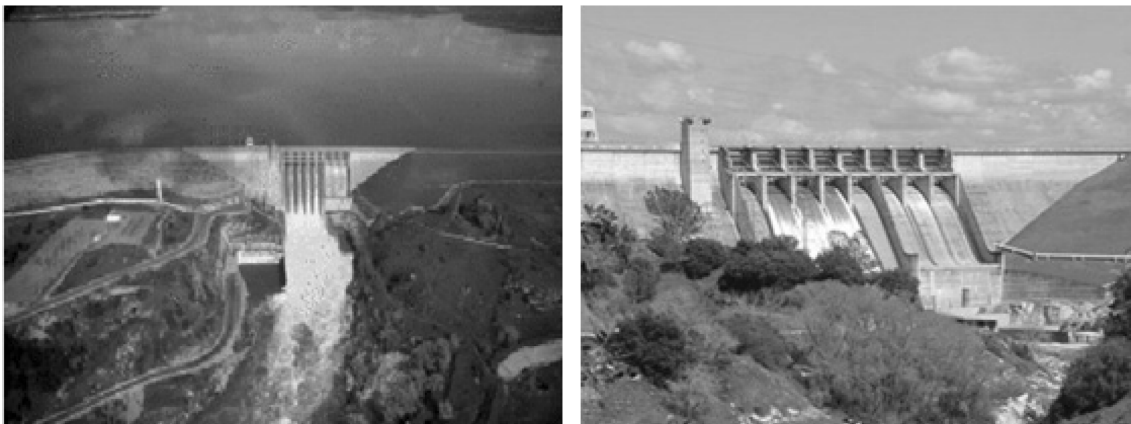
Fig. 5 Pictures of Folsom dam (http://www.usbr.gov/dataweb/dams/ca10148.htm 2007)
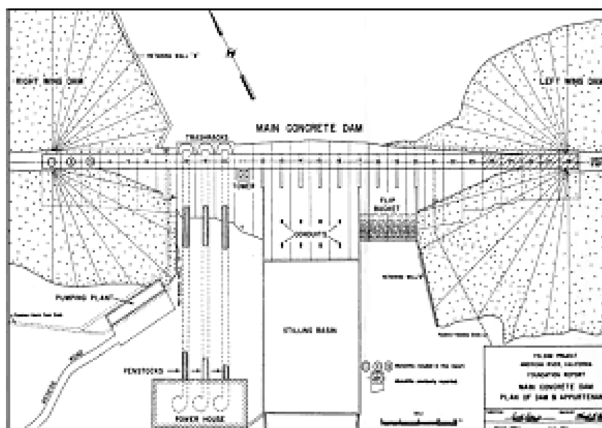
Fig. 6 Plan view of Folsom dam (US Army Corps of Engineers 2003)
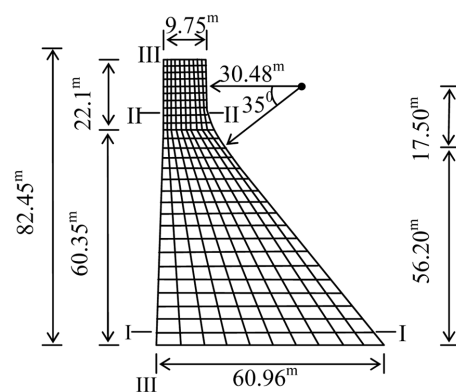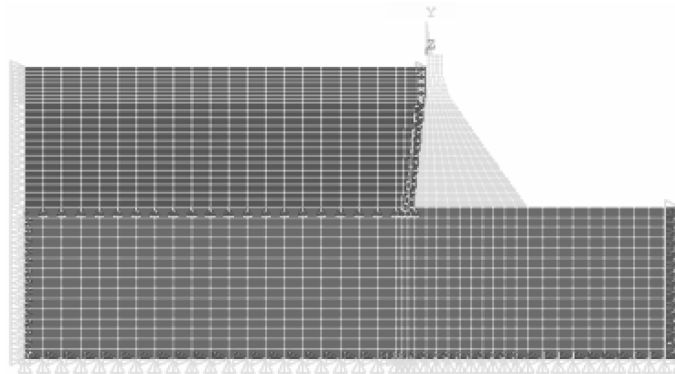
Fig. 7 Geometry of monolith 21

Fig. 8 The two dimensional finite element model of Folsom gravity dam

Table 3 Material properties for Folsom gravity dam (US Army Corps of Engineers 2003)

Material	Material properties				
	Modulus of elasticity N/m^2	Poisson's ratio	Mass per unit Vol. kg/m^3	Cohesion N/m^2	Friction angle
Dam (Concrete)	4.068E10	0.19	2530	3E6	35
Foundation	5.424E10	0.30	-	-	-
Reservoir	207E7	-	1000	-	-

lifts and founded in hard granodiorite rock. Monoliths 1 through 11 are referred to as the right gravity section, Monoliths 12 through 20 as the spillway section, and Monoliths 21 through 28 as the left gravity section (Fig. 6). Geometry and relevant dimensions of monoliths 21 are presented in Fig. 7 (US Army Corps of Engineers 2003).

Four significant faults were identified beneath the concrete gravity section during construction. Two parallel faults, termed the Penstock and Wingwall Faults, were exposed beneath Monoliths 4-6. These faults were found to strike in an upstream-downstream direction and dip 30 to 45 deg NW (US Army Corps of Engineers 2003).

The finite element model including dam-reservoir-foundation interaction of Folsom gravity dam is shown in Fig. 8. The values of the material properties used for the model are shown in Table 3. The values of elasticity modulus and the Poisson's ratios considered in this study are taken from US Army Corps of Engineers (2003).
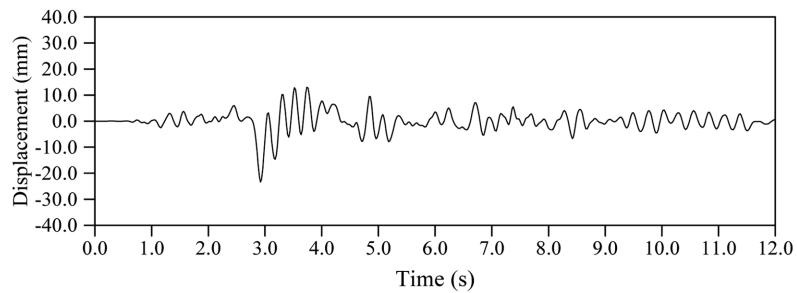
4.1.1 Displacements

The time histories of horizontal displacements (upstream-downstream direction) at the crest point of Folsom gravity dam obtained from non-linear analysis subjected to each ground motion is presented Figs. 9(a)-(c). The maximum displacements at this point subjected to Duzce, Erzincan and Northridge ground motions are 28 mm, 24 mm and 33 mm, respectively. Although Duzce ground motion has the peak acceleration value, the maximum values of displacement are obtained from Northridge earthquake ground motion.
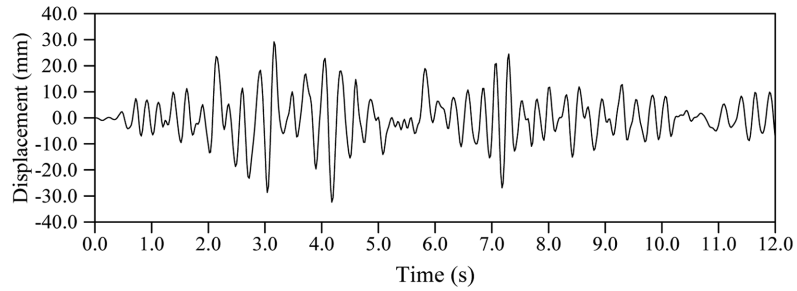
The variation of displacements with height of Folsom gravity dam subjected to Duzce 1999,
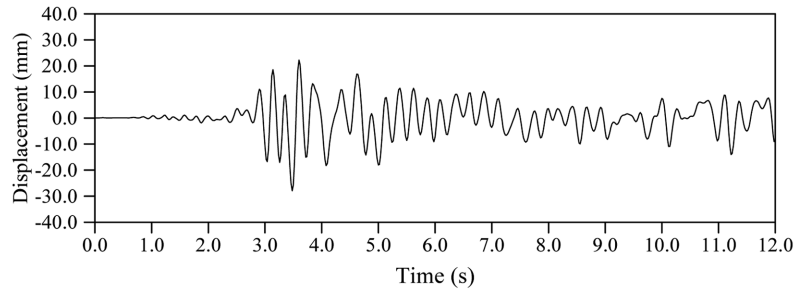
(a) The time histories of horizontal displacements subjected to Duzce 1999

(b) The time histories of horizontal displacements subjected to Erzincan 1992

(c) The time histories of horizontal displacements subjected to Northridge 1994

Fig. 9 The time histories of horizontal displacements at the crest of Folsom gravity dam
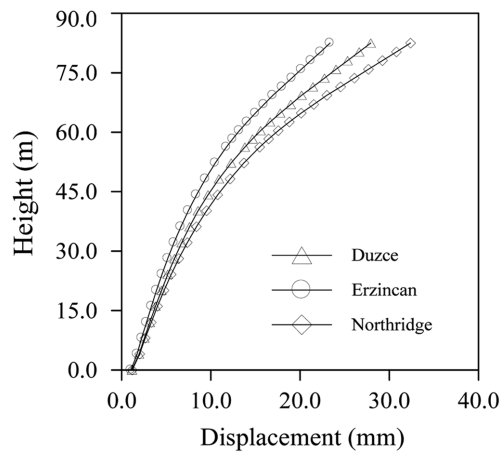

Fig. 10 Maximum horizontal displacements along the height of Folsom gravity dam

Erzincan 1992 and Northridge 1994 earthquake ground motions are denoted in Fig. 10. It is clearly seen that horizontal displacements increase along the height of the dam and displacements obtained from Northridge earthquake ground motion are the highest.

4.1.2 Principal stresses

The maximum compressive and tensile principal stresses received from I-I, II-II, and III-III section in Fig. 7, respectively, are shown subjected to each ground motion in Figs. 11-13. The values of the maximum compressive and tensile principal stresses attained from Duzce, Erzincan, and Northridge earthquakes ground motions are given in Table 4. In all sections, maximum compressive and tensile principal stresses obtained from Northridge earthquake ground motion are the highest. The stresses which are captured from section I-I are higher than section II-II, so it can
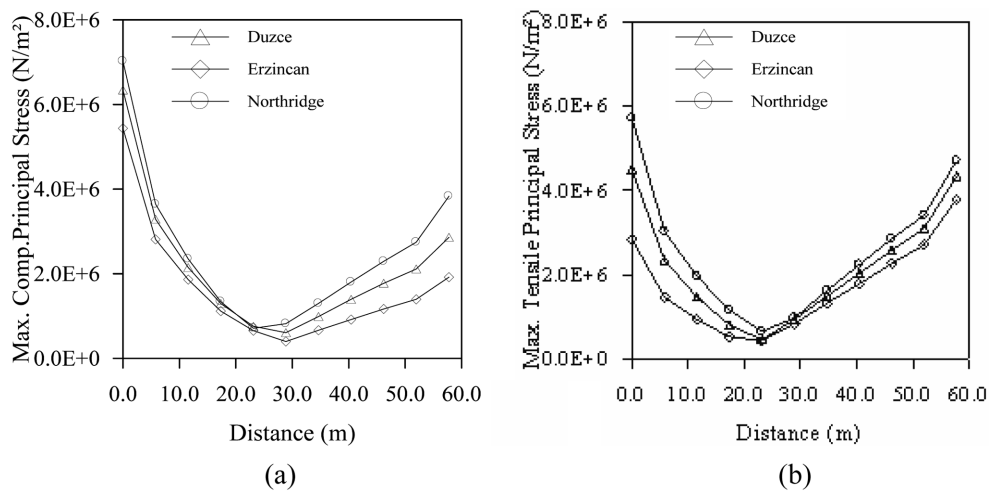
Fig. 11 (a) The maximum compressive and (b) tensile principal stresses at section I-I
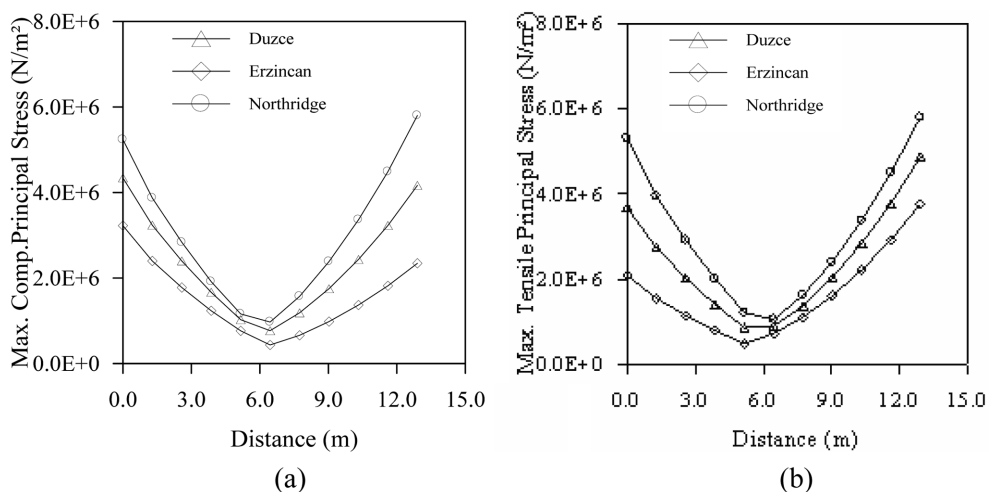
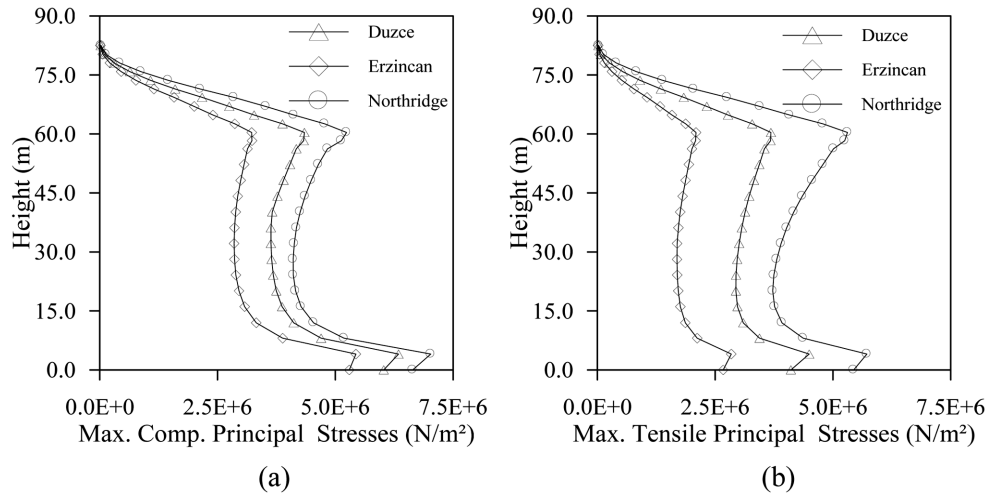Fig. 12 (a) The maximum compressive and (b) tensile principal stresses at section II-II

Fig. 13 (a) The maximum compressive and (b) tensile principal stresses at section III-III

Table 4 The maximum compressive and tensile principal stresses

Earthquake	I-I Section		II-II Section		III-III Section	
	MCPS[1] (MPa)	MTPS[2] (MPa)	MCPS (MPa)	MTPS (MPa)	MCPS (MPa)	MTPS (MPa)
Duzce	6.34	4.49	4.34	3.68	6.34	4.49
Erzincan	5.43	2.84	3.22	2.09	5.43	2.84
Northridge	7.02	5.72	5.24	5.31	7.02	5.72

[1]MCPS: Maximum Compressive Principal Stress.
[2]MTPS: Maximum Tensile Principal Stress.

be said that stresses towards the bottom of structure are higher than upper sides.

The time histories of the maximum and minimum principal stresses of Folsom gravity dam subjected to Duzce 1999, Erzincan 1992 and Northridge 1994 earthquake-ground motions are plotted in Figs. 14(a)-(c). It can easily be comprehended by the figures below that maximum and minimum principal stresses, which are obtained from Folsom gravity dam, are the highest for Northridge 1994 earthquake ground motion and these values subjected to Duzce 1999 earthquake ground motion are higher than the ones subjected to Erzincan 1992 earthquake ground motion.

4.2 Earthquake response of arch dam

A double curvature Type-5 arch dam suggested in "Arch Dams" symposium in England in 1968 is selected (Arch Dams 1968). Type-5 arch dam model is developed including reservoir and foundation. The geometric properties and 3-D model of Type-5 arch dam is given in Fig. 15.

The height of the dam is 120 m and the computed thicknesses of the dam at the top and base are 5.35 m and 23.35 m, respectively. View of the dam-reservoir-foundation system is given in Figs. 16, 17. There are three unknown displacements at each nodal point in dam, foundation and reservoir finite element model. The values of the material properties used for the dam model in this study are presented in Table 5.
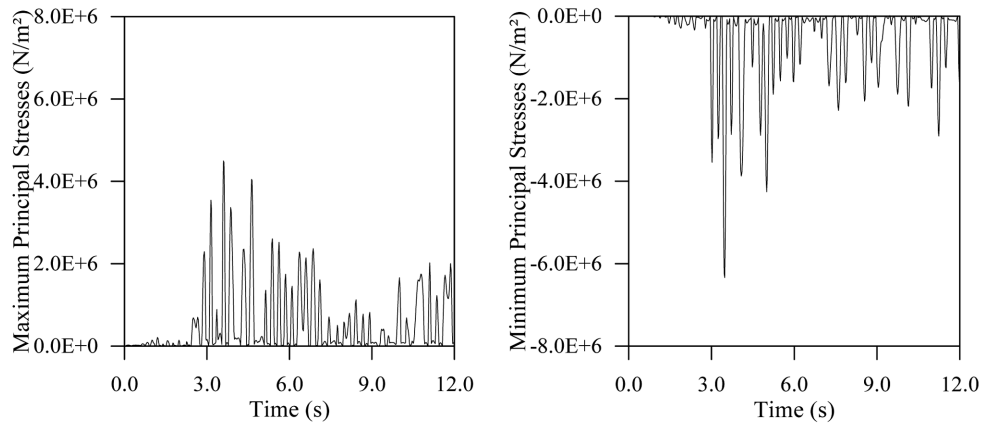
(a) The maximum and minimum principal stresses subjected to Duzce 1999
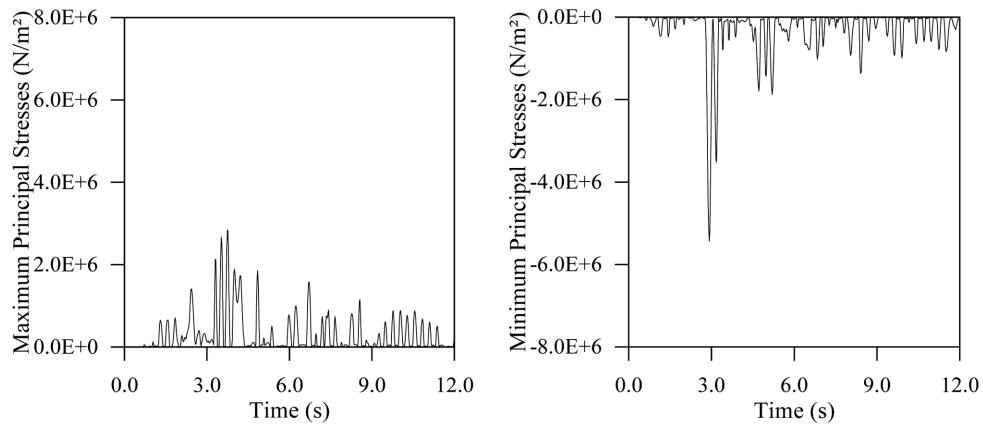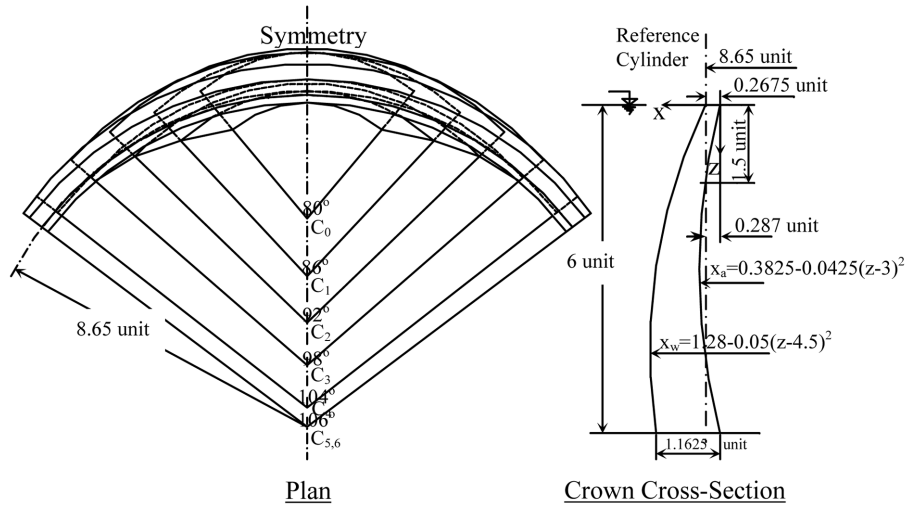

(b) The maximum and minimum principal stresses subjected to Erzincan 1992
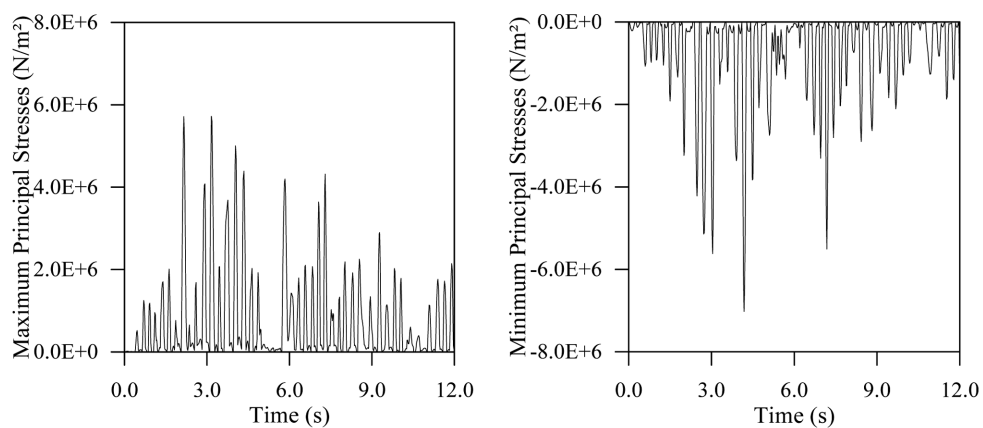
(c) The maximum and minimum principal stresses subjected to Northridge 1994

Fig. 14 The maximum and minimum principal stresses for Folsom gravity dam

Level	C_0	C_1	C_2	C_3	C_4	C_5	C_6
Radius (unit)	3.67	5.29	6.64	7.72	8.54	8.80	8.50
Central Angle	80°	86°	92°	98°	104°	106°	106°

Fig. 15 Plan view and vertical crown cross section of Type-5 arch dam
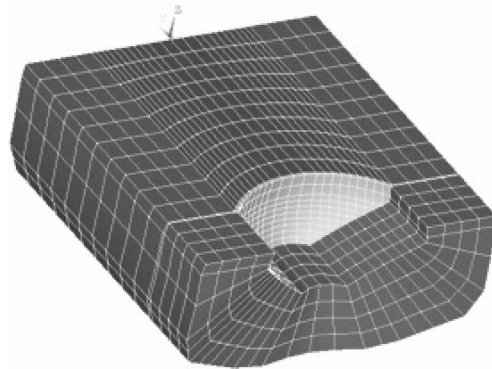
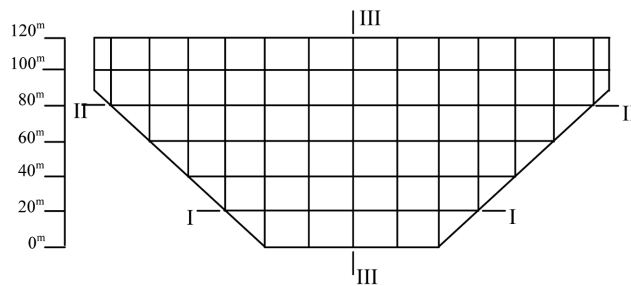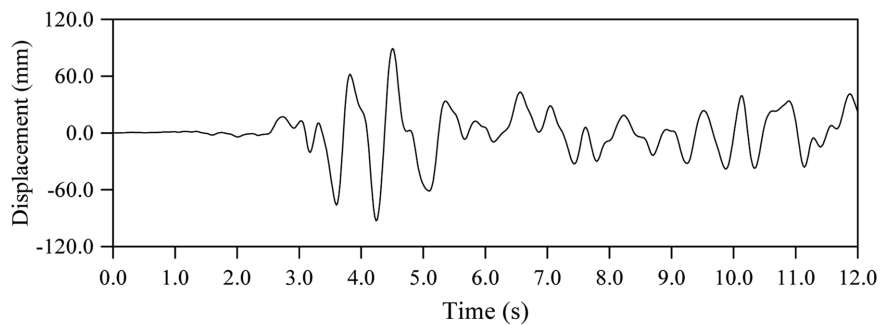Fig. 16 Three dimensional finite element model of Type-5 arch dam

Fig. 17 Finite element mesh of Type-5 arch dam

Table 5 Material properties for Arch dam

Material	Material properties				
	Modulus of elasticity	Poisson's ratio	Mass per unit Vol.	Cohesion	Friction angle
	N/m^2		kg/m^3	N/m^2	
Dam (Concrete)	3.310E10	0.152	2476	3E6	35
Foundation	2.100E10	0.30	-	-	-
Reservoir	207E7	-	1000	-	-

(a) The time histories of horizontal displacements subjected to Duzce 1999
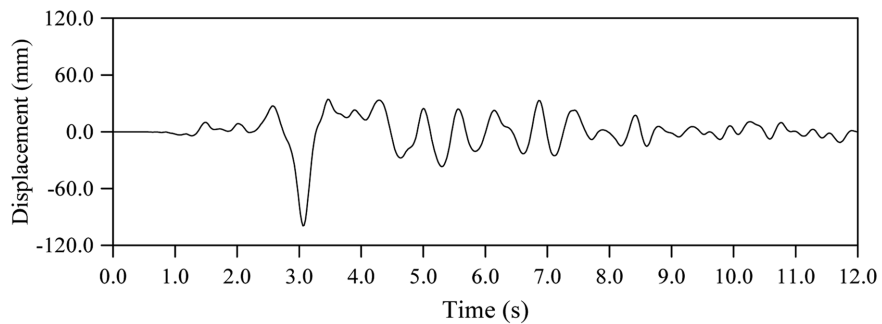
(b) The time histories of horizontal displacements subjected to Erzincan 1992
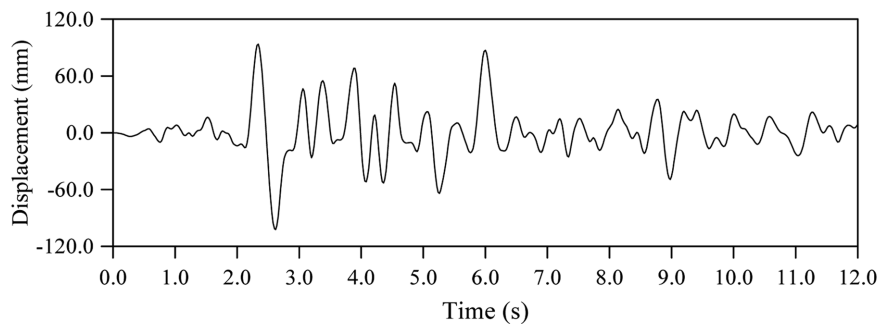
(c) The time histories of horizontal displacements subjected to Northridge 1994

Fig. 18 The time histories of horizontal displacements at the crest of Type-5 arch dam
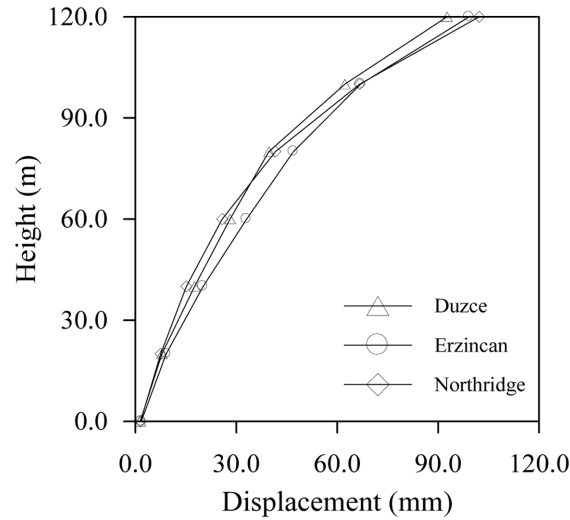
Fig. 19 Maximum horizontal displacements along the height of Type-5 arch dam

4.2.1 Displacements

The time histories of horizontal displacements (upstream-downstream direction) at the crest point of Type-5 Arch dam obtained from non-linear analysis subjected to each ground motion are presented in Figs. 18(a)-(c). The maximum displacements on this point subjected to Duzce, Erzincan and Northridge ground motions are 92.61 mm, 99.19 mm and 102.16 mm, respectively. Although Duzce ground motion has the peak acceleration value, the maximum values of displacement is obtained from Northridge earthquake ground motion. In addition, the horizontal displacements attained from Duzce 1999 earthquake ground motion are the lowest.

The variation of displacements with height of Type-5 arch dam subjected to Duzce 1999, Erzincan 1992 and Northridge 1994 earthquakes ground motions are obtained in Fig. 19. It is obviously seen that horizontal displacements increase along the height of the dam and maximum displacement occurs under Northridge earthquake ground motion. It is also indicated that the displacements, which are procured from Erzincan earthquake ground motion, are higher than the others till 20-25 m from the crest point of the dam.

4.2.2 Principal stresses

The maximum compressive and tensile principal stresses obtained from I-I, II-II, and III-III section in Fig. 17, respectively, are given subjected to each ground motion in Figs. 20-22. The maximum compressive and tensile principal stresses resulted from Duzce, Erzincan, and Northridge earthquake ground motions are yielded in Table 6. In section I-I, in spite of the maximum compressive principal stresses are attained from the Erzincan earthquake ground motion, the maximum tensile stresses occur under Northridge earthquake. In section II-II, maximum compressive principal stresses are relatively close to each other. Maximum tensile principal stresses resulted from Duzce and Northridge earthquake ground motions are fairly close, however these values at Erzincan earthquake ground motion are smaller than the others. In section III-III, maximum compressive and tensile principal stresses have changeable.

The time histories of maximum and minimum principal stresses of Type-5 arch dam subjected to
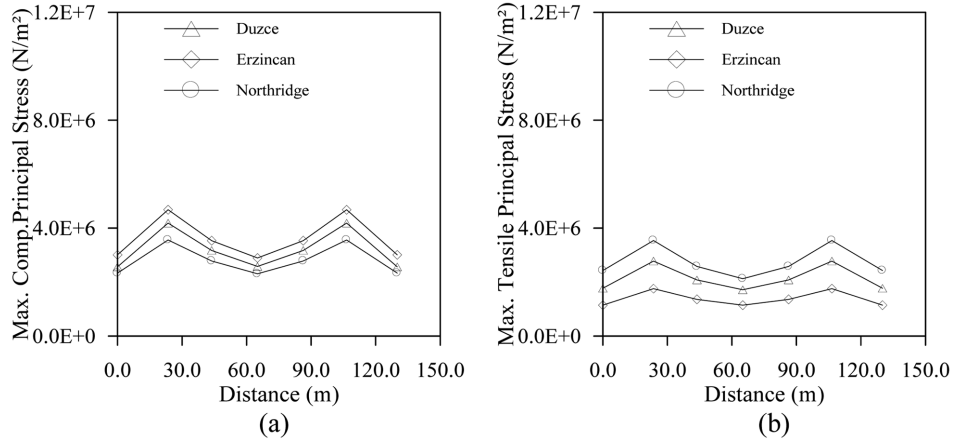
Fig. 20 (a) The maximum compressive and (b) tensile principal stresses at section I-I
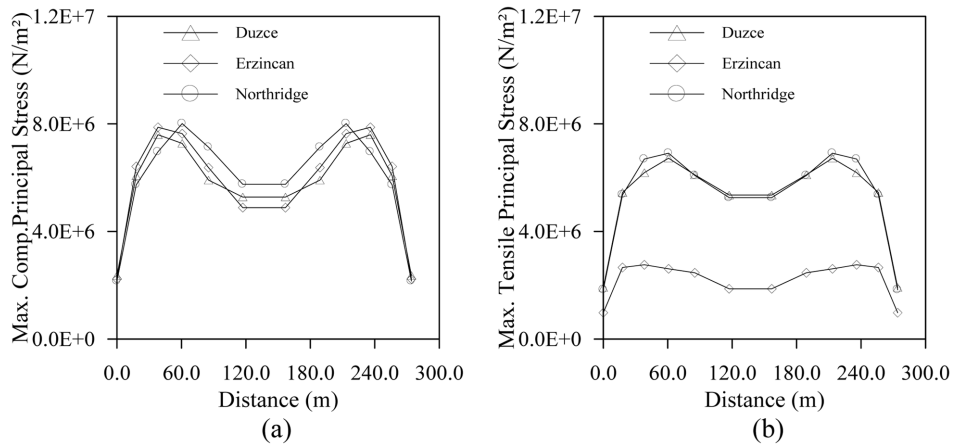

Fig. 21 (a) The maximum compressive and (b) tensile principal stresses at section II-II
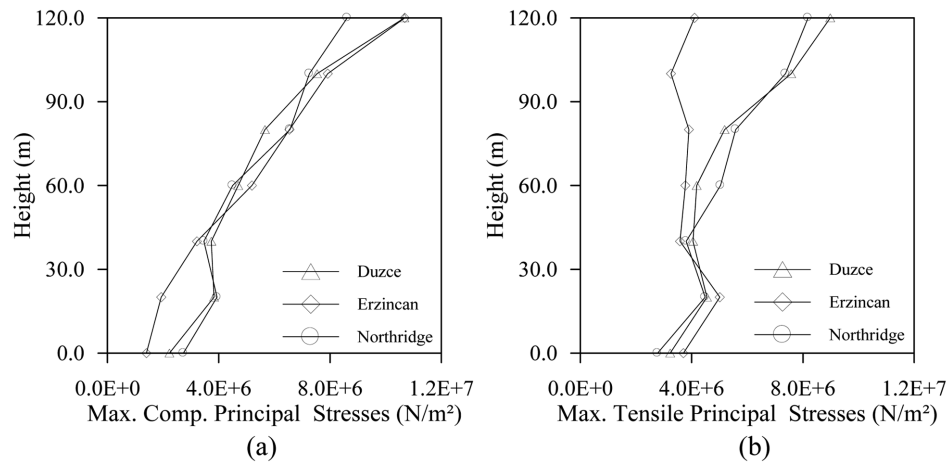

Fig. 22 (a) The maximum compressive and (b) tensile principal stresses at section III-III

Table 6 The maximum compressive and tensile principal stresses

| Earthquake	I-I Section		II-II Section		III-III Section	
	MCPS[1] (MPa)	MTPS[2] (MPa)	MCPS (MPa)	MTPS (MPa)	MCPS (MPa)	MTPS (MPa)
Duzce	4.18	2.78	7.60	6.72	10.67	8.98
Erzincan	4.68	1.76	7.88	2.76	10.68	5.01
Northridge	3.56	3.58	8.01	6.91	8.62	8.13

[1]MCPS: Maximum Compressive Principal Stress
[2] MTPS: Maximum Tensile Principal Stress
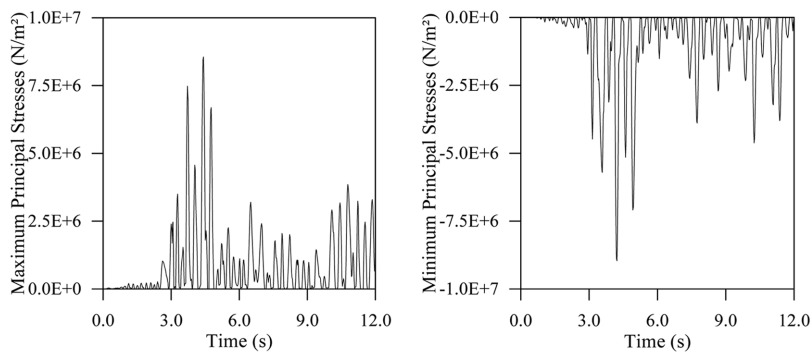
(a) The maximum and minimum principal stresses subjected to Duzce 1999
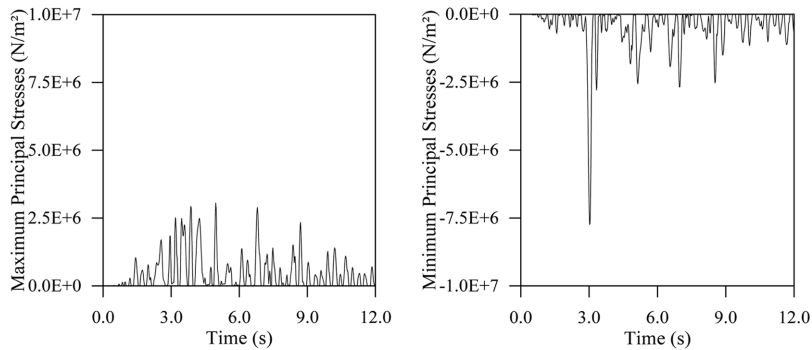
(b) The maximum and minimum principal stresses subjected to Erzincan 1992
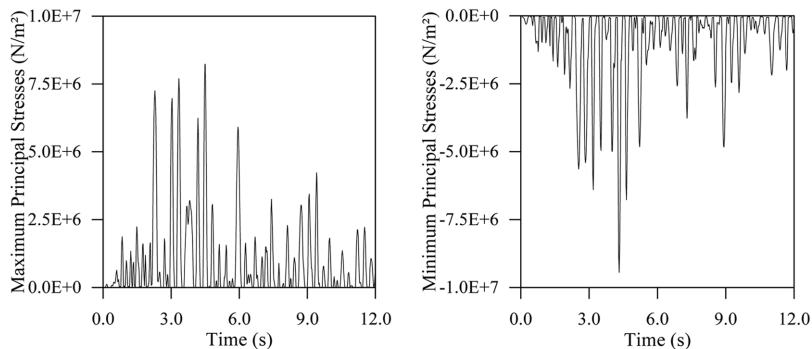
(c) The maximum and minimum principal stresses subjected to Northridge 1994

Fig. 23 The maximum and minimum principal stresses for Type-5 arch dam

Duzce 1999, Erzincan 1992 and Northridge 1994 earthquake ground motions, respectively, are demonstrated in Fig. 23(a)-(c). It is inferred from the below figures that while maximum principal stresses form in Duzce earthquake ground motion, minimum principal stresses are revealed in Northridge earthquake ground motion.

4.3 Earthquake response of concrete faced rockfill dam

Torul Dam, located approximately 14 km northwest of Torul, Gumushane, has been still constructed since 2000 by General Directorate of State Hydraulic (Fig. 24). It has been established on Harsit River. This dam was projected as a concrete faced rockfill dam. The reservoir will be used for power-generation purpose. The dam crest is 320 m length and 12 m wide, and the maximum height and base width are 142 m and 420 m, respectively. The dam consists of concrete face slab, 2A, 3A, 3B, 3C and 3D regions from upstream face to downstream face. The two
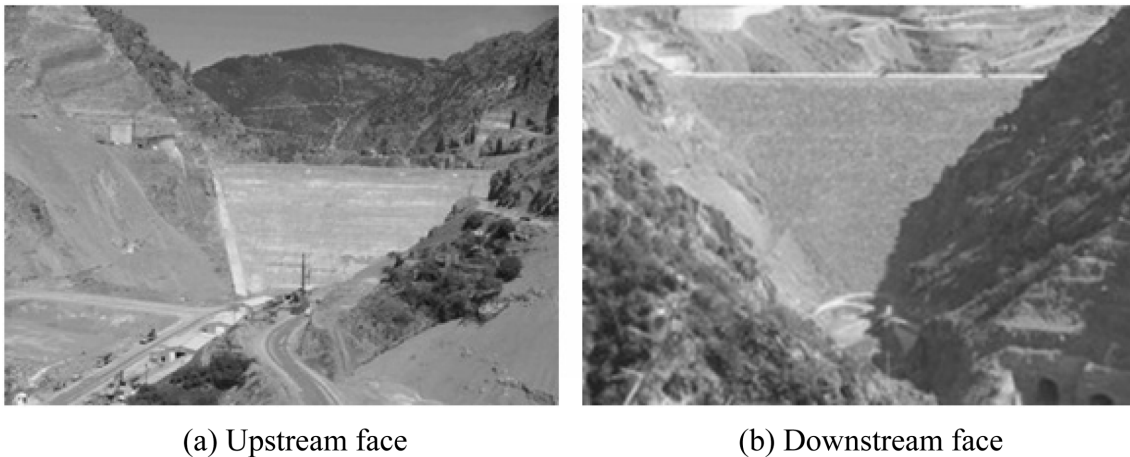
(a) Upstream face   (b) Downstream face

Fig. 24 The view of Torul concrete faced rockfill dam (DSI 2006)
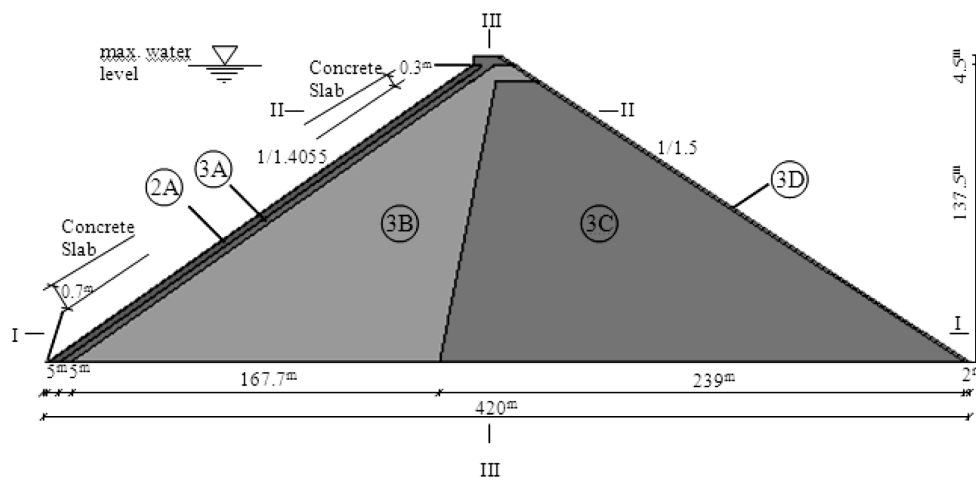

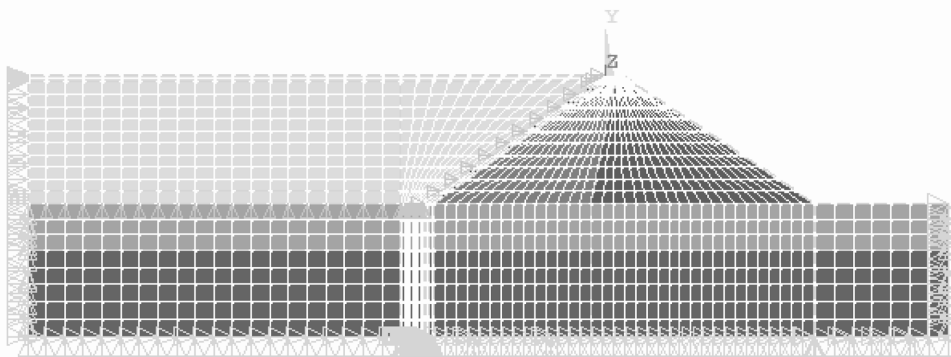Fig. 25 Two dimensional largest cross section of Torul dam (DSI 2006)

Fig. 26 The two dimensional finite element model of Torul concrete faced rockfill dam

Table 7 Material properties for Torul concrete faced rockfill dam

| Material	D_{max} (mm)	Material properties				
		Modulus of elastisity	Poisson's ratio	Mass per unit Vol.	Cohesion	Frict. angle
		N/m^2		kg/m^3	N/m^2	
Concrete	-	2.850E10	0.18	2395.5	3E6	35
2A (sifted rock or allivium)	150	1.400E10	0.26	2905.2	3E6	35
3A (selected rock)	300	1.350E10	0.26	2854.2	3E6	35
3B (filling with quarry rock)	600	1.250E10	0.26	2833.8	3E6	35
3C (filling with quarry rock)	1000	1.150E10	0.26	2803.3	3E6	35
3D (selected rock)	2000	1.100E10	0.26	2752.3	3E6	35
Foundation (Diabase)	-	0.840E10	0.40	-	-	-
Foundation (Granodiorite)	-	1.155E10	0.40	-	-	-
Reservoir	-	207E7	-	1000	-	-

dimensional largest cross section and some dimensions of the dam are demonstrated in Fig. 25. The concrete slab-rockfill interface is modelled as welded contact and contact allowing slippage. If welded contact is used, concrete slab and rockfill have the same nodes in common interface on contrary to contact allowing slippage. In this study, welded contact was taken into account.

The finite element models including dam-reservoir-foundation interaction of Torul concrete faced rockfill dam is shown in Fig. 26. The modeling procedure in Torul dam is considered as used in Folsom gravity dam.

The values of the material properties used for the dam model in this study are shown in Table 7. The values of elasticity modulus and the Poisson's ratios considered in this study are taken from the project of the dam.
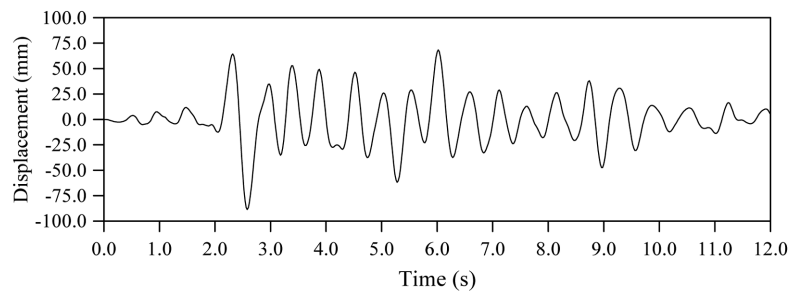
4.3.1 Displacements

The time histories of horizontal displacements (upstream-downstream direction) at the crest point of Torul concrete faced rockfill dam obtained from non-linear analysis subjected to each ground motions are presented Figs. 27(a)-(c). The maximum horizontal displacement at this point subjected
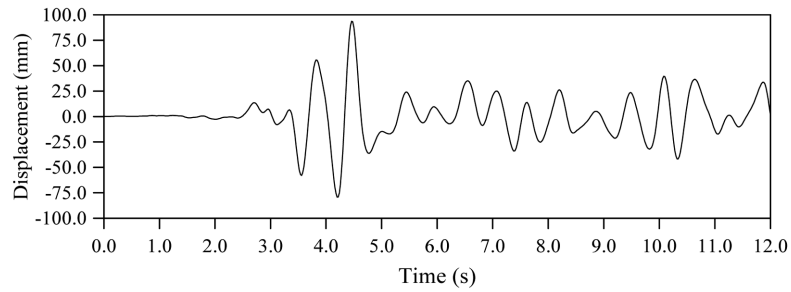
(a) The time histories of horizontal displacements subjected to Duzce 1999
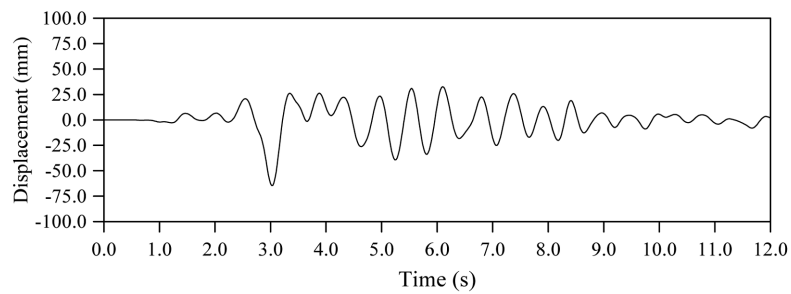
(b) The time histories of horizontal displacements subjected to Erzincan 1992

(c) The time histories of horizontal displacements subjected to Northridge 1994

Fig. 27 The time histories of horizontal displacements at the crest point of Torul concrete faced rockfill dam
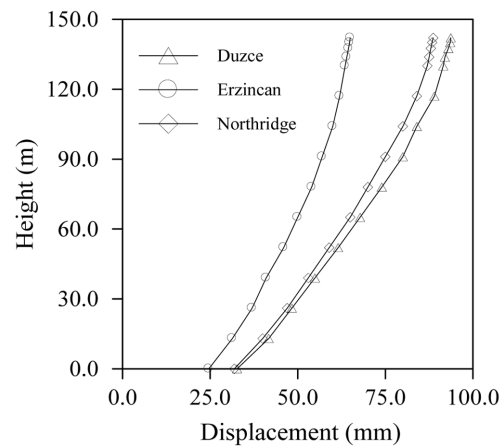

Fig. 28 Maximum horizontal displacements along the height of Torul concrete faced rockfill dam

to Duzce, Erzincan and Northridge ground motions occur 93.65 mm, 65 mm and 88.65 mm, respectively. Duzce near-fault strong ground motion has both the peak acceleration value and the maximum values of displacements.

The variation of displacements with height of Torul concrete faced rockfill dam subjected to Duzce 1999, Erzincan 1992 and Northridge 1994 earthquake ground motions are shown in Fig. 28. It is understood from the figure that horizontal displacements increase along the height of the dam and displacements obtained from Duzce earthquake ground motion are the highest.

4.3.2 Principal stresses

The maximum compressive and tensile principal stresses obtained from I-I, II-II, and III-III section in Fig. 25, respectively, are given in Figs. 29-31 subjected to each ground motion. The maximum compressive and tensile principal stresses caused by Duzce, Erzincan, and Northridge earthquakes ground motions are shown in Table 8. In all sections, despite the maximum compressive principal stresses are resulted from Northridge earthquake ground motion, maximum
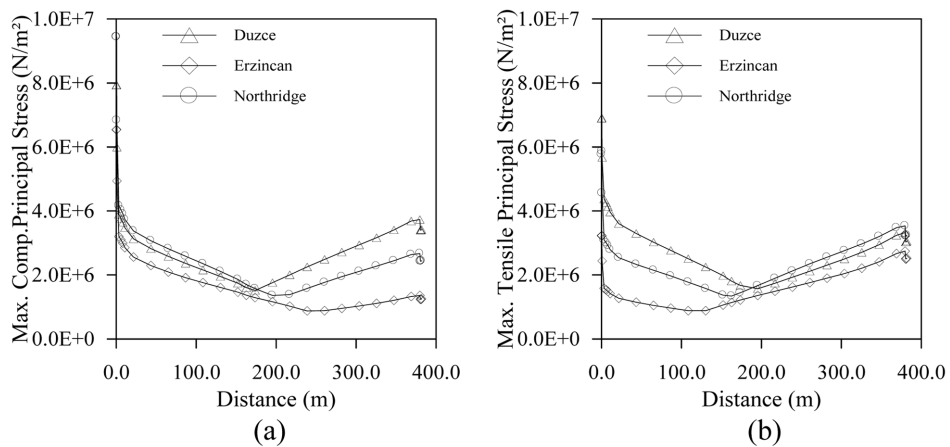

Fig. 29 (a) The maximum compressive and (b) tensile principal stresses at section I-I
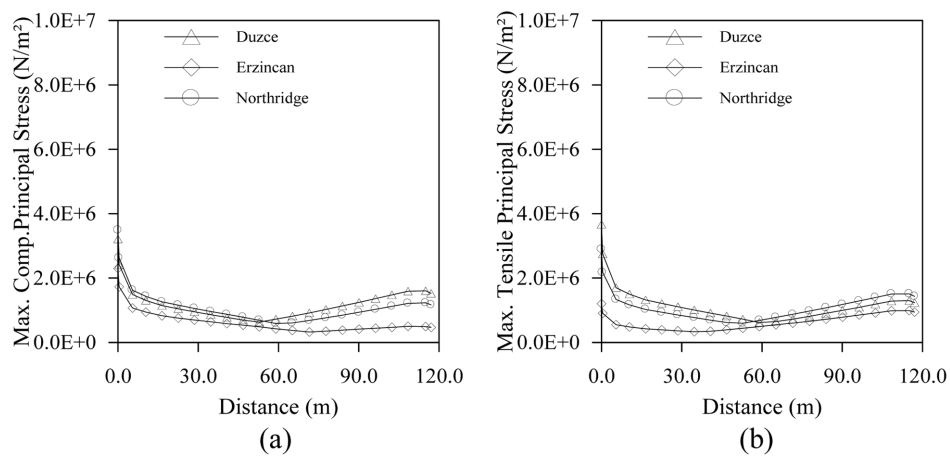

Fig. 30 (a) The maximum compressive and (b) tensile principal stresses at section II-II
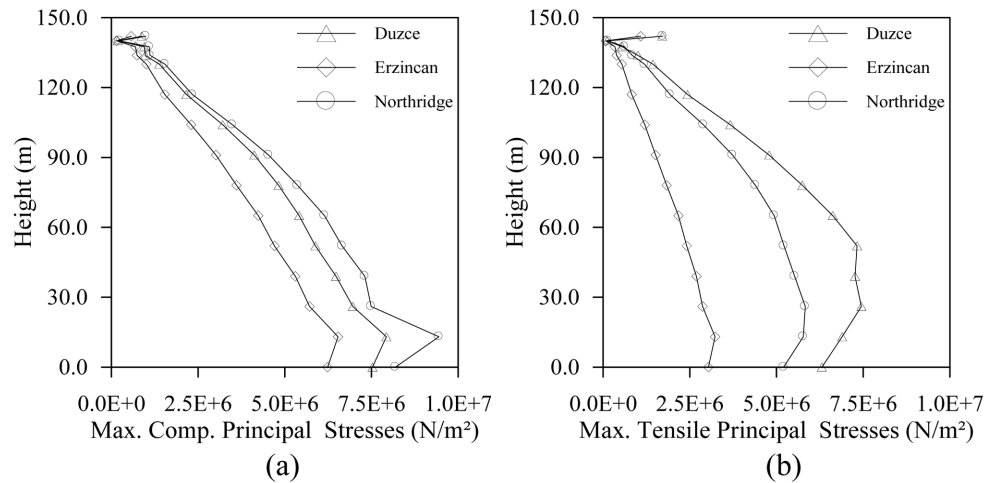
Fig. 31 (a) The maximum compressive and (b) tensile principal stresses at section III-III

Table 8 The maximum compressive and tensile principal stresses

Earthquake	I-I Section		II-II Section		III-III Section	
	MCPS[1] (MPa)	MTPS[2] (MPa)	MCPS (MPa)	MTPS (MPa)	MCPS (MPa)	MTPS (MPa)
Duzce	7.936	6.901	3.209	3.664	7.928	7.446
Erzincan	6.541	3.229	2.298	1.202	6.534	3.225
Northridge	9.442	5.865	3.485	2.890	9.442	5.826

[1]MCPS: Maximum Compressive Principal Stress
[2]MTPS: Maximum Tensile Principal Stress

tensile principal stresses are generally attained from Duzce earthquake ground motion. It is obviously seen that maximum compressive and tensile principal stresses have a decreasing trend by height from bottom to top of dam.

The time histories of maximum (tensile) and minimum (compression) principal stresses of Torul concrete faced rockfill dam subjected to Duzce 1999, Erzincan 1992 and Northridge 1994 earthquake ground motions, respectively is obtained in Figs. 32(a)-(c). The maximum principal stresses have come into being in Duzce earthquake ground motion, yet the minimum principal stresses have occurred in Northridge earthquake ground motion.

4.4 Earthquake response of clay core rockfill dam

Kose Dam, located approximately 3 km northwest of Kose town, Gumushane, has been still constructed since 1996 by General Directorate of State Hydraulic (Fig. 33). It has been established on Kose River. This dam was projected as a clay core rockfill dam. The reservoir will be used for irrigation purpose. The dam crest is 316 m length and 12 m wide, and the maximum height and base width are 81 m and 336 m, respectively. The two dimensional largest cross section and some dimensions of the dam are demonstrated in Fig. 34.

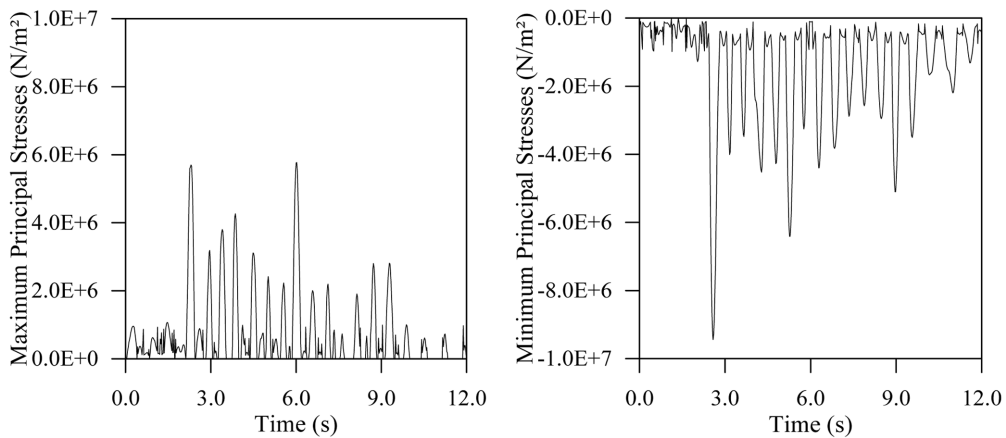The finite element models including dam-reservoir-foundation interaction of Kose clay core
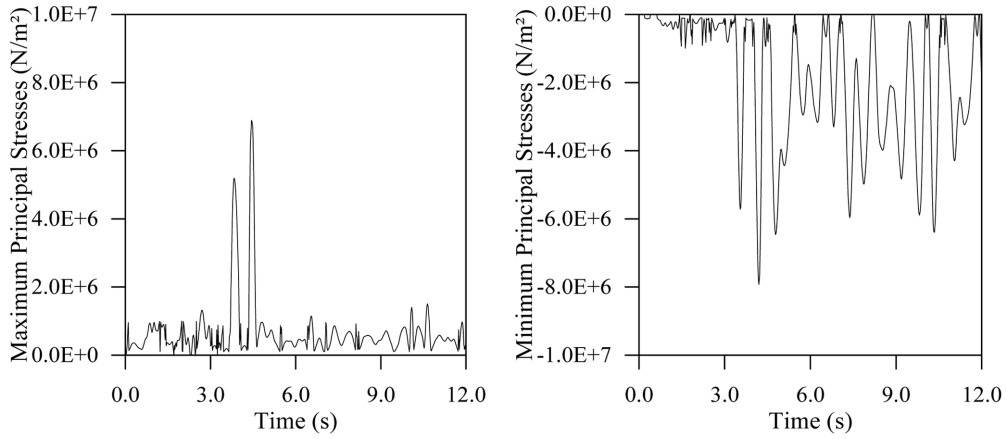
(a) The maximum and minimum principal stresses subjected to Duzce 1999
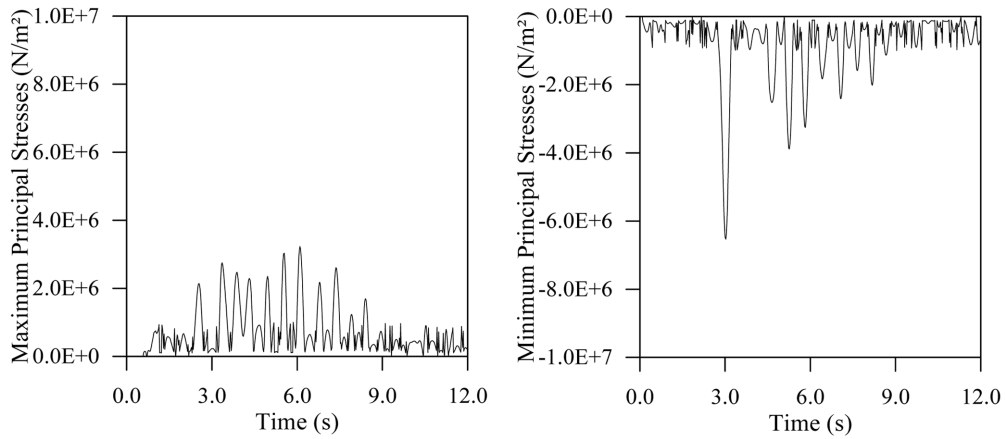
(b) The maximum and minimum principal stresses subjected to Erzincan 1992

(c) The maximum and minimum principal stresses subjected to Northridge 1994

Fig. 32 The maximum and minimum principal stresses for Torul Concrete Faced Rockfill dam

(a) Upstream face of Kose dam   (b) Downstream face of Kose dam

Fig. 33 Some views from Kose clay core rockfill dam (DSI 2006)

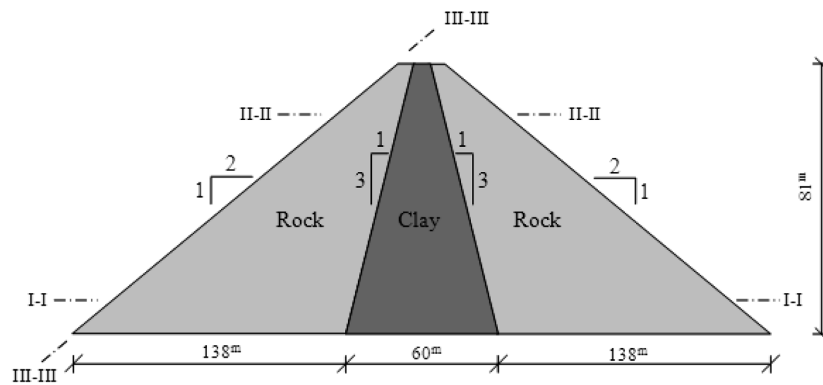Fig. 34 Two dimensional largest cross section of Kose dam (DSI 2006)
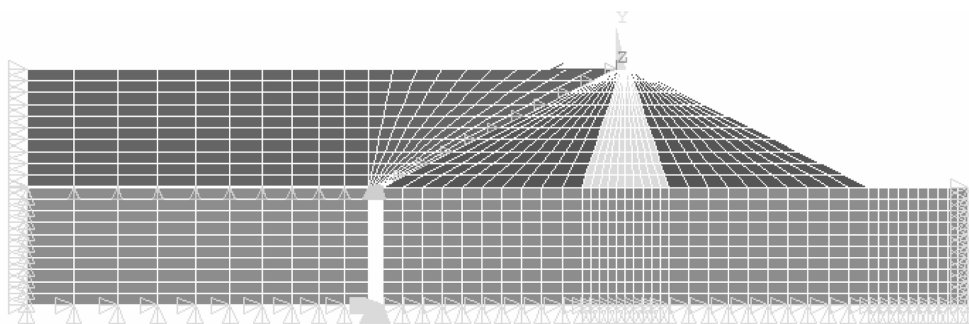

Fig. 35 The two dimensional finite element model of Kose clay core rockfill dam

rockfill dam is shown in Fig. 35.

The values of the material properties used for the dam model in this study are shown in Table 9. The values of elasticity modulus and the Poisson's ratios considered in this study are taken from the projects of the dam.

Table 9 Material properties for Kose clay core rockfill dam

Material	Material properties				
	Modulus of Elasticity	Poisson's ratio	Mass per unit Vol.	Cohesion	Friction angle
	N/m^2		kg/m^3	N/m^2	
Dam (Clay)	1.015E10	0.45	2089.7	3E6	35
Dam (Rock)	1.632E10	0.36	2120.3	-	-
Foundation	1.379E10	0.24	-	-	-
Reservoir	207E7	-	1000	-	-
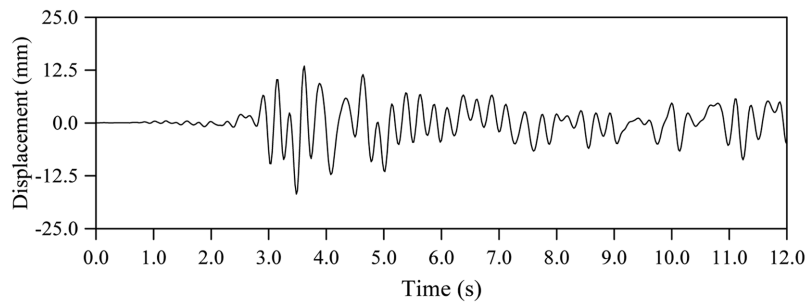
(a) The time histories of horizontal displacements subjected to Duzce 1999
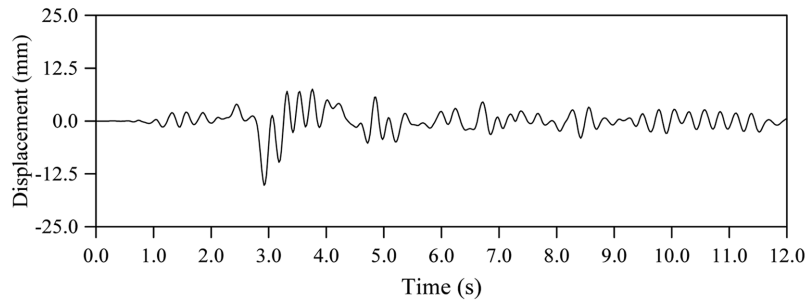
(b) The time histories of horizontal displacements subjected to Erzincan 1992
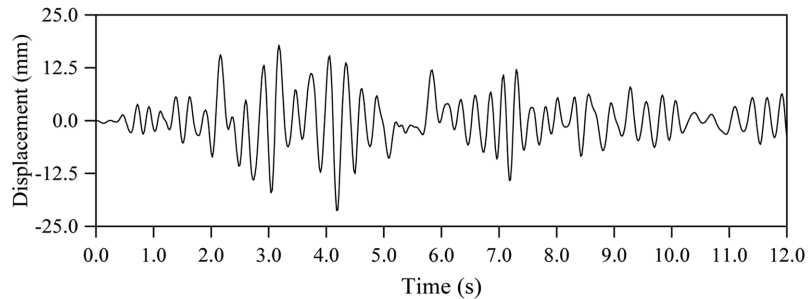
(c) The time histories of horizontal displacements subjected to Northridge 1994

Fig. 36 The time histories of horizontal displacements at the crest of Kose clay core rockfill dam

Fig. 37 Maximum horizontal displacements along the height of Kose clay core rockfill dam

4.4.1 Displacements

The time histories of horizontal displacements (upstream-downstream direction) at the crest point of Kose clay core rockfill dam obtained from non-linear analysis subjected to each ground motion is presented in Figs. 36(a)-(c). The maximum horizontal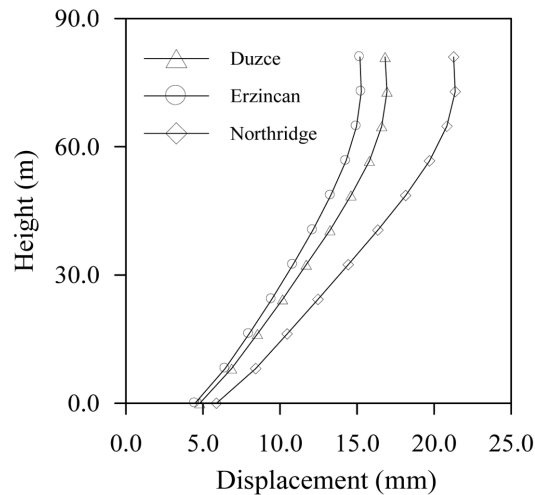 displacements on this point subjected to Duzce, Erzincan and Northridge ground motions are 16.82 mm, 15.19 mm and 21.27 mm, respectively. The maximum value of the displacement has been attained from Northridge earthquake ground motion, although Duzce ground motion has the peak acceleration value.

The variation of displacements with height of Kose clay core rockfill dam subjected to Duzce 1999, Erzincan 1992 and Northridge 1994 earthquake ground motions are shown in Fig. 37. It can easily be seen in Fig. 37 that the horizontal displacements increase along the height of the dam and that those corresponding to Northridge earthquake ground motion are the highest.

4.4.2 Principal stresses

The maximum compressive and tensile principal stresses obtained from I-I, II-II, and III-III section in Fig. 34 are given in Figs. 38-40 subjected to each ground motion. The maximum compressive and tensile principal stresses obtained from Duzce, Erzincan, and Northridge earthquake ground motions are submitted in Table 10. In all sections, maximum compressive and tensile principal stresses obtained from Northridge earthquake ground motion are the highest. Stresses which are obtained from section I-I are higher than section II-II, so it can be appeared that stresses towards the bottom of structure are higher than upper sides.

The time histories of maximum and minimum principal stresses of Kose clay core rockfill dam subjected to Duzce 1999, Erzincan 1992 and Northridge 1994 earthquake ground motions, respectively are given in Figs. 41(a)-(c). From that Fig. 41, maximum principal stresses, which are attained from Duzce and Erzincan earthquake ground motions, are close to each other; however these are the highest in Northridge earthquake ground motion. The minimum principal stresses considering the values have occurred in Northridge, Duzce, and Erzincan earthquakes ground motions, respectively.
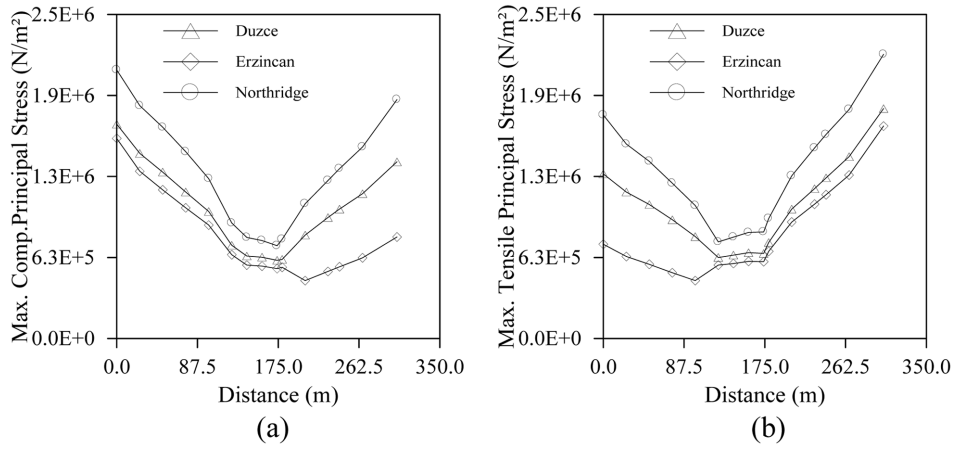
Fig. 38 (a) The maximum compressive and (b) tensile principal stresses at section I-I
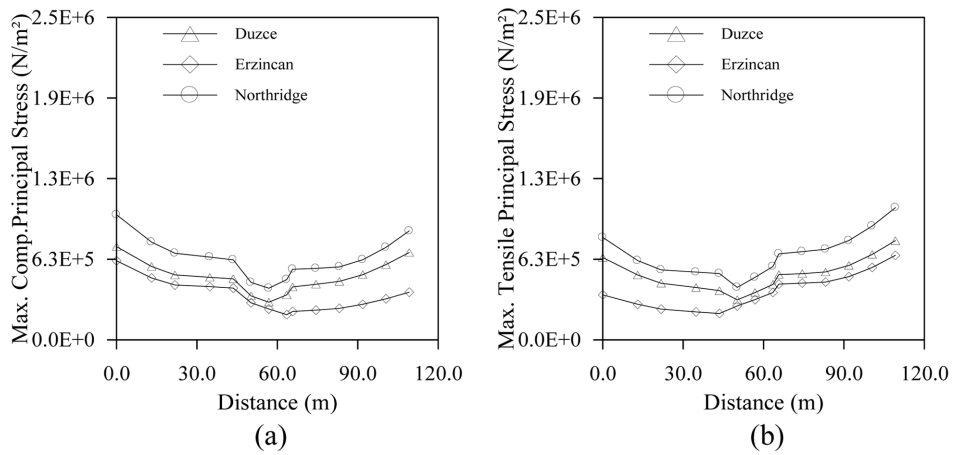

Fig. 39 (a) The maximum compressive and (b) tensile principal stresses at section II-II
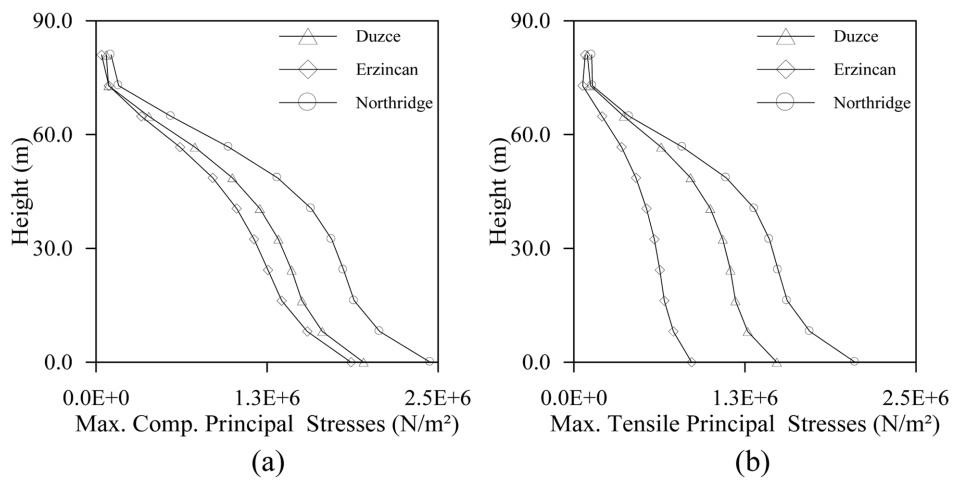
Fig. 40 (a) The maximum compressive and (b) tensile principal stresses at section III-III

Table 10 The maximum compressive and tensile principal stresses

Earthquake	I-I Section		II-II Section		III-III Section	
	MCPS[1] (MPa)	MTPS[2] (MPa)	MCPS (MPa)	MTPS (MPa)	MCPS (MPa)	MTPS (MPa)
Duzce	1.653	1.403	0.723	0.769	1.955	1.483
Erzincan	1.543	1.639	0.613	0.655	1.864	0.861
Northridge	2.073	2.193	0.970	1.025	2.443	2.056

[1] MCPS: Maximum Compressive Principal Stress
[2] MTPS: Maximum Tensile Principal Stress
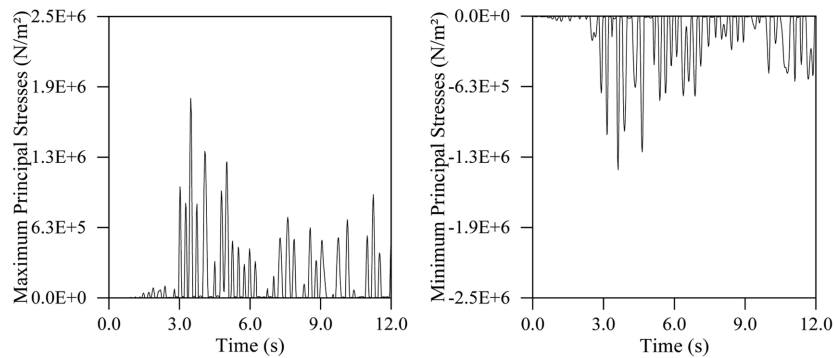
(a) The maximum and minimum principal stresses subjected to Duzce 1999
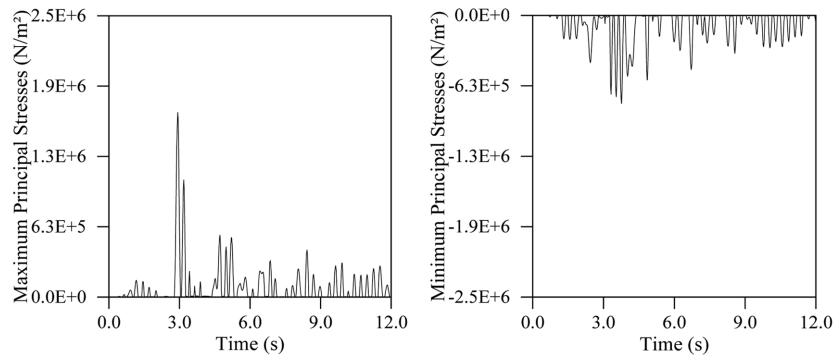
(b) The maximum and minimum principal stresses subjected to Erzincan 1992
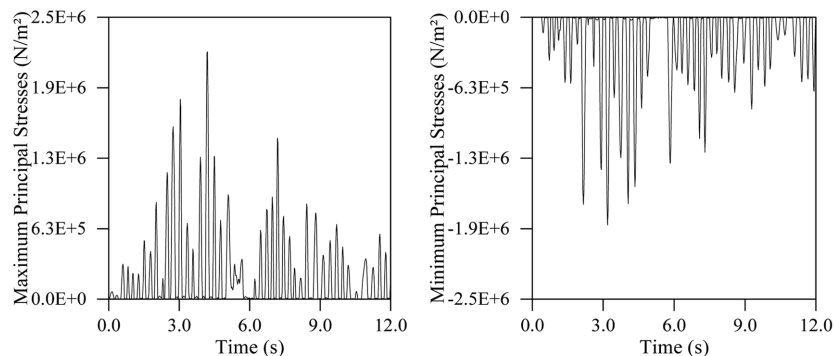
(c) The maximum and minimum principal stresses subjected to Northridge 1994

Fig. 41 The maximum and minimum principal stresses for Kose clay core rockfill dam

5. Conclusions

The effects of the near-fault strong ground motions on the nonlinear behaviors of dams involving dam-reservoir-foundation interaction by using Lagrangian approach were studied in this paper. Nonlinear transient analyses were performed on Folsom gravity dam, double curvature Type-5 arch dam, Torul concrete faced rockfill dam, and Kose clay core rockfill dam. For each dam model, Duzce (1999), Northridge (1994), and Erzincan (1992) near-fault strong ground motion records which have close amplitudes were taken into account separately. The nonlinear displacements and stresses are calculated and compared with each other.

The displacements increase with height of all dam types. Maximum compressive and tensile principal stresses have a decreasing trend by height from bottom to top of concrete gravity, concrete faced rock fill and clay core rock fill dams. Maximum compressive and tensile principal stresses have changeable from bottom to top of arch dam.

Although Duzce ground motion has the peak acceleration value, the maximum values of displacements and stresses are obtained from Northridge earthquake ground motion for clay core rockfill, concrete gravity and arch dams. However, the results obtained from Duzce earthquake ground motion for concrete faced rock fill dam are higher than the others.

It is seen that maximum displacements and principal stresses have not occurred anytime when near-fault earthquake has peak acceleration value.

It is seen from the conclusions of this study that different near-fault strong ground motion records should be considered in the dynamic nonlinear transient analysis of dams.

References

Agrawal, A.K. and He, W.-L. (2002), "A closed-form approximation of near-fault ground motion pulses for flexible structures", *15th ASCE Engineering Mechanics Conference*, New York.

Aki, K. (1968), "Seismic displacement near a fault", *J. Geophys. Res.*, **64**, 321-342.

Akkas, N., Akay, H.U. and Ylmaz, C. (1979), "Applicability of general-purpose finite element programs in solid-fluid interaction problems", *Comput. Struct.*, **10**, 773-783.

Anderson, J.C. and Bertero, V.V. (1987), "Uncertainties in establishing design earthquakes", *J. Struct. Eng.*, **113**, 1709-1724.

ANSYS (2003), Swanson Analysis System, US.

Araujo, J.M. and Awruch, A.M. (1998), "Probabilistic finite element analysis of concrete gravity dams", *Adv. Eng. Software*, **29**, 97-104.

Arch Dams (1968), A Review of British Research and Development, *Proc. of the Symposium Held at the Institution of Civil Engineers*, London, England.

Archuleta, R.J. and Hartzell, S.H. (1981), "Effect of fault finiteness on near-source ground motion", *Bull. Seism. Soc. Am.*, **71**, 939-957.

Bathe, K.J. (1996), *Finite Element Procedures in Engineering Analysis*, Englewood Cliffs, New Jersey, Prentice-Hall.

Bayraktar, A., Dumanolu, A.A. and Calayr, Y. (1996), "Asynchronous dynamic analysis of dam-reservoir-foundation systems by the Lagrangian approach", *Comput. Struct.*, **58**, 925-935.

Bayraktar, A., Hancer, E. and Akköse, M. (2005), "Influence of base-rock characteristics on the stochastic dynamic response of dam-reservoir-foundation systems", *Eng. Struct.*, **27**, 1498-1508.

Bayraktar, A., Hancer, E. and Dumanolu, A.A. (2005), "Comparison of stochastic and deterministic dynamic responses of gravity dam-reservoir systems using fluid finite elements", *Finite Elem. Anal. Des.*, **41**, 1365-1376.

Bertero, V.V., Mahin, S.A. and Herrera, R.A. (1978), "A seismic desing implications of near-fault San Fernando earthquake records", *Earthq. Eng. Struct. D.*, **6**, 31-42.

Bray, J.D. and Marek, A.R. (2004), "Characterization of forward-directivity ground motions in the near-fault region", *Soil D. Earthq. Eng.*, **24**, 815-828.

Calayr, Y. (1994), Dynamic Analysis of Concrete Gravity Dams using the Eulerian and Lagrangian Approaches, Ph.D. Thesis, Karadeniz Technical University, Trabzon, Turkey, (in Turkish).

Calayr, Y., Dumanolu, A.A. and Bayraktar, A. (1996), Earthquake analysis of gravity dam-reservoir systems using the Eulerian and Lagrangian approaches", *Comput. Struct.*, **59**, 877-890.

Chopra, A.K. (1968), "Earthquake behavior of reservoir-dam systems", *J. Eng. Mech. Div.*, 1475-1500.

Chopra, A.K. and Chakrabarti, P. (1981), "Earthquake analysis of concrete gravity dams including dam-water-foundation rock interaction", *Earthq. Eng. Struct. D.*, **9**, 363-383.

Chopra, A.K. and Chintanapakdee, C. (2001), "Comparing response of SDF systems to near-falt and far-fault earthquake motions in the context of spectral regions", *Earthq. Eng. Struct. D.*, **30**, 1769-1789.

Clough, R.W. and Penzien, J. (1975), *Dynamics of Structures*, McGraw-Hill, New York.

Corigliano, M., Lai, C.G. and Barla, G. (2006), "Seismic response of rock tunnels in near-fault conditions", *First European Conference on Earthquake Engineering and Seismology*, Switzerland.

Dicleli, M. and Buddaram, S. (2006), "Equivalent linear analysis of seismic-isolated bridges subjected to near-fault ground motions with forward rupture directivity effect", *Eng. Struct.*, (in press).

DSI (2006), General Directorate of State Hydraulic, Ankara, Turkey, http://www.dsi.gov.tr/english/.

Fenves, G. and Chopra, A.K. (1984), "Earthquake analysis of concrete gravity dams including reservoir bottom absorption and dam-water-foundation rock interaction", *Earthq. Eng. Struct. D.*, **12**, 663-680.

Fenves, G. and Chopra, A.K. (1984), "Earthquake analysis of concrete gravity dams including reservoir bottom absorption and dam-water-foundation rock interaction", *Earthq. Eng. Struct. D.*, **12**, 663-680.

Finn, W.D.L. and Varolu, E. (1973), "Dynamics of gravity dam-reservoir systems", *Comput. Struct.*, **3**, 913-924.

Galal, K. and Ghobarah, A. (2006), "Effect of near-fault earthquakes on North American nuclear design spectra", *Nucl. Eng. Des.*, **236**, 1928-1936.

Ghahari, F., Jahankhah, H. and Ghannad, M.A. (2006), "The effect of background record on response of structures subjected to near-fault ground motions", *First European Conference on Earthquake Engineering and Seismology*, Switzerland.

Greeves, E.J. (1991), "The modeling and analysis of linear and nonlinear fluid-structure systems with particular reference to concrete dams", Ph.D. Thesis, Department of Civil Engineering, University of Bristol, Bristol.

Greeves, E.J. and Dumanolu, A.A. (1989), "The implementation of an efficient computer analysis for fluid-structure interaction using the Eulerian approach within SAP-IV", Department of Civil Engineering, University of Bristol, Bristol.

Hall, J.F., Heaton, T.H., Halling, M.W. and Wald, D.J. (1995), "Near-source ground motion and its effects on flexible buildings", *Earthq. Spectra*, **11**, 569-605.

http://www.usbr.gov/dataweb/dams/ca10148.htm, 2007.

Liao, W.-I., Loh, C.-H. and Lee, B.-H. (2004), "Comparison of dynamic response of isolated and non-isolated continuous girder bridges subjected to near-fault ground motions", *Eng. Struct.*, **26**, 2173-2183.

Makris, N. (1997), "Rigidity-plasticity-viscosity: Can electrorheological dampers protect baseisolated structures from near-source ground motions?", *Earthq. Eng. Struct. D.*, **26**, 571-591.

Megawati, K., Higashihara, H. and Koketsu, K. (2001), "Derivation of near-source ground motions of the 1995 Kobe (Hyogo-ken Nanbu) earthquake from vibration records of the Akashi Kaikyo Bridge and its implications", *Eng. Struct.*, **23**, 1256-1268.

Ozturk, B. (2006), "A simple procedure for the assessment of seismic drift response of building structures located in seismically active and near-fault regions", *First European Conference on Earthquake Engineering and Seismology*, Switzerland.

PEER (Pacific Earthquake Engineering Research Centre) (2006), http://peer.berkeley.edu/smcat/data.

Pulido, N. and Kubo, T. (2004), "Near-fault strong motion complexity of the 2000 Tottori earthquake (Japan) from a broadband source asperity model", *Tectonophysics*, **390**, 177-192.

Saini, S.S., Bettess, P. and Zienkiewicz, O.C. (1978), "Coupled hydrodynamic response of concrete gravity dams using finite and infinite elements", *Earthq. Eng. Struct. D.*, **6**, 363-374.

Singhal, A.C. (1991), "Comparison of computer codes for seismic analysis of dams", *Comput. Struct.*, **38**, 107-112.

Somerville, P.G. (2003), "Magnitude scaling of the near fault rupture directivity pulse", *Phys. Earth Planet. In.*, **137**, 201-212.

Somerville, P.G., Smith, N.F., Graves, R.W. and Abrahamson, N.A. (1997), "Abrahamson, Modification of empirical strong ground motion attenuation relations to include the amplitude and duration effects of rupture directivity", *Seismic. Res. Lett.*, **68**, 199-222.

US Army Corps of Engineers (2003), Time-history dynamic analysis of concrete hydraulic h-structures, Engineering and Design.

Wang, G-Q., Zhou, X.-Y., Zhang, P.-Z. and Igel, H. (2002), "Characteristics of amplitude and duration for near fault strong ground motion from the 1999 Chi-Chi, Taiwan earthquake", *Soil D. Earthq. Eng.*, **22**, 73-96.

Wilson, E.L. and Khalvati, M. (1983), "Finite elements for the dynamic analysis of fluid-solid systems", *Int. J. Numer. Meth. Eng.*, **19**, 1657-1668.

Zangar, C.N. and Haefei, R.J. (1952), "Electric analog indicates effects of horizontal earthquake shock on dams", *Civil Eng.*, **4**, 54-55.

Zienkiewicz, O.C. and Nath, B. (1963), "Earthquake hydrodynamic pressures on arch dams-an electric analogue solution", *In Proc. of Int. Civil Eng. Congress*, **25**, 165-176.